University of Alberta

The Production and Characterization of Cellulose Nanofibrils

by

Yang Gao

A thesis submitted to the Faculty of Graduate Studies and Research
in partial fulfillment of the requirements for the degree of

Master of Science
in
Chemical Engineering

Chemical and Materials Engineering

Fall 2013
Edmonton, Alberta

To my dear sister:

Tina Gao

Abstract

In this thesis, a cellulose nanofibril (CNF) preparation method in the biorefinery platform is described, and the product is characterized and compared to commercially available varieties. CNF is a bundle of cellulose microfibrils with diameter in 5-100 nanometer range and length reaching to micrometer range. The development of value-added co-products is critical for the economic viability of biorefineries which convert biomass to commodity fuels. The raw materials used are two pulps from the NSERC Bioconversion Network. The biomass was converted to CNF by shear mixing and multiple mechanical shearing through a microfluidizer. The produced CNF's viscous properties, morphology and stability were characterized and compared against two commercially available varieties. The CNF produced from organosolv pulp is a high surface area material with superior viscous properties, and it has great potential in viscosity modification applications.

Acknowledgement

The author would like to acknowledge the guidance in research and thesis preparation of supervisor Dr. Yaman Boluk and co-supervisor Dr. Phillip Choi. This research was supported by the University of Alberta and NSERC Bioconversion Network. I thank the National Institute for Nanotechnology and Alberta Innovates – Technology Futures for providing training and research equipment. I also thank Daicel FineChem Ltd. and Innventia AB for supplying CNF samples, and Mascoma Inc. for supplying pulp samples. The organosolv pulping was done by Dr. Richard Chandra and the descriptions of the process were written by Dr. Chandra with few editions. The scanning electron microscopy of commercial samples was performed by Dr. Usha Hemraz, and dynamic light scattering of commercial samples were performed by Dr. Christophe Danumah.

Table of contents

List of tables

List of figures

List of abbreviations

CNF	-	cellulose nanofibrils
MP	-	mechanical pulp
OP	-	organosolv pulp
DLS	-	dynamic light scattering
G'	-	storage modulus
G"	-	loss modulus
MP	-	mechanical pulp
STEM	-	scanning transmission electron microscopy

1. Introduction

Cellulose is the most plentiful biopolymer on Earth, and it has been utilized by humans since ancient times.[1] The main sources for cellulose are wood, which is the most abundant, and cotton, which has high cellulose content.[2] The primary structure of cellulose is shown in Figure 1-1.

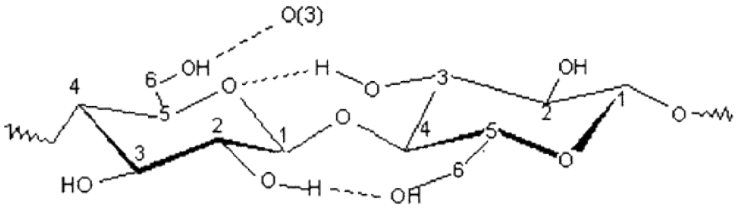

Figure 1-1 – Cellulose molecular structure[3]

In cellulose primary structure, the glucose monomers are linked by β-1→4 glycosidic bonds, which are called glucan chains. The secondary structure of cellulose consists of parallel glucan chains bundled together by hydrogen bonds, giving cellulose its stiffness.[4] In plant cells, cellulose is mainly found in the S2 layer of cell walls.[5] A diagram of S2 composition is shown in Figure 1-2.

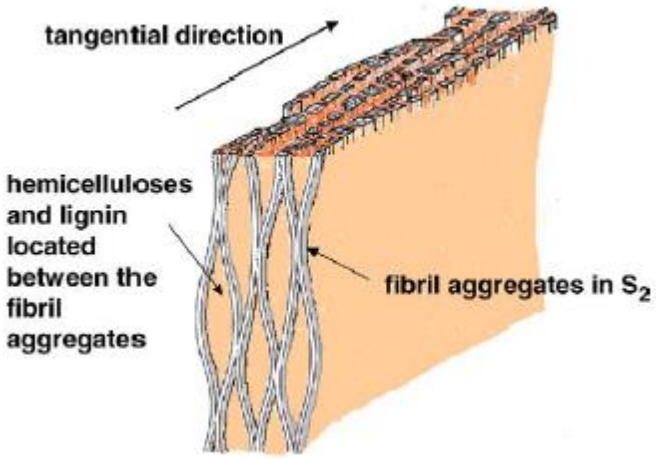

Figure 1-2 – Cell wall S2 structure with cellulose, lignin and hemicellulose[5]

As seen in Figure 1-2, cellulose is entwined with hemicelluloses and lignin. Glucan chains form cellulose microfibrils that are 3-4 nm in diameter, and the microfibrils bundle to form cellulose aggregates that are 16-20 nm.[5] In order to make functional cellulose polymers, the cellulose needs to be liberated from the structure. Cellulose has been made into functional polymers at an industrial scale as early as 1870, when celluloid was produced by Hyatt Manufacturing Company.[1] Since then, many cellulose derivatives have been produced, such as rayon and methylcellulose.[2, 6]

The increased pollution emissions in the world has led to research efforts in utilizing renewable resources. Cellulosic biomass is a natural resource that can be converted to biofuel and bioproducts. Biomass processing yields many environmental benefits: CO_2 capture from photosynthesis, biodegradability and

renewability. Although the biofuel/bioproducts industry is not yet self-sufficient in Canada, bioethanol has gained a significant market in Brazil.[7] A major roadblock in cellulose ethanol production is the recalcitrance of lignocellulosic material, making expensive pretreatments necessary.[7]

Paper and pulp has traditionally been the largest or sector of the forestry industry in North America by wood consumption.[8] In this age of digitization, it is unsurprising that paper consumption has decreased 4 % between 2001-2007 in North America according to The International Union of Forest Research Organizations.[8] For example, newsprint consumption in the US took a sharp dip from 2005 as seen in Figure 1-3.

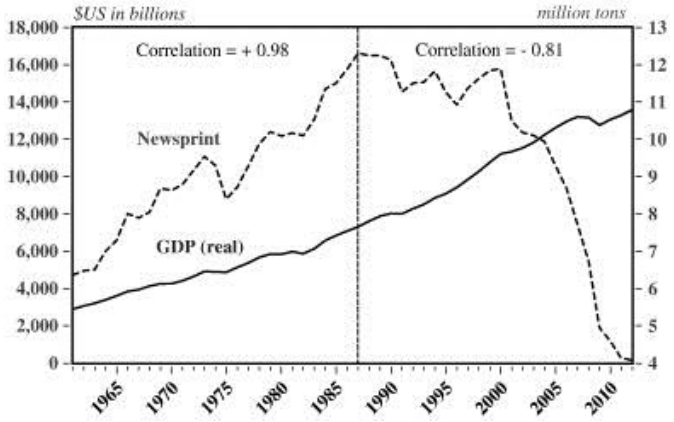

Figure 1-3 – Newsprint consumption and GDP in the US from 1961 to 2012[9]

Additionally, paper recycling has increased dramatically world-wide, causing the decrease the demand for new paper and pulp.[8] Since paper and pulp has been such a large contributor to the forestry industry in North America, alternative uses for

wood and pulp such as cellulose nanocrystals and cellulose nanofibrils are being explored.[2]

Cellulose nanofibrils (CNF) is a cellulose derivative that is gaining interest as a green, renewable material.[2] CNF was first reported by Turbak et al in 1984.[10] CNFs are very thin and long fibres, with diameters of 10-100 nm and length in micrometer scale.[2] CNFs have high surface area, higher interaction, light-weight, green and inexpensive.[2, 11] The TAPPI standard nomenclature is CNF, but it is also known as nanofibrillated cellulose (NFC) and microfibrillated cellulose (MFC).[2, 12]

This study is funded by the NSERC Bioconversion Network, which is a national research and development network that focuses on converting wood biomass to biofuel and other valuable products.[13] Figure 1-4 shows how the Bioconversion Network operates.

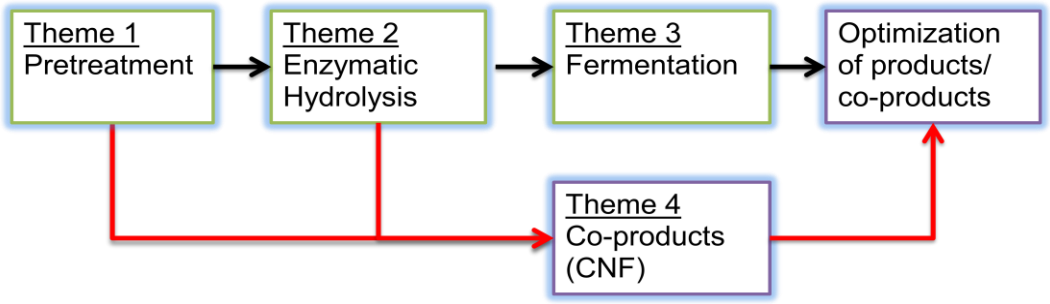

Figure 1-4 – NSERC Bioconversion Network diagram

In Theme 1, wood is pretreated by mechanical or chemical means to form pulp. In Theme 2, the pulp is enzymatically hydrolyzed to produce glucose. The fermentation of glucose into ethanol biofuel is explored in Theme 3. In Theme 4, the production of other valuable co-products is explored. Pulp from Theme 1 and leftover biomass from enzymatic hydrolysis in Theme 2 are both explored as feedstock material for the co-products in Theme 4. The production of CNF falls into Theme 4 – co-products, and the red arrows in Figure 1-4 indicate how other sections of the network collaborate with Theme 4. CNF can be a value-added co-product within the biorefinery platform. Incorporating CNF into the expensive biorefing process can bring added revenue and adds to the economic viability of biorefineries. [14]

CNF can be produced by mechanical, enzymatic, chemical and dissolution/electrospinning methods.[2, 15] The size and morphology of CNF can be characterized with dynamic light scattering, electron microscopy and atomic force

microscopy.[16] CNF is shear thinning, which means its viscosity decreases as shear rate increases. [2] The viscous properties of CNF in steady state and oscillation can be characterized by a rheometer.[16] CNF is suitable for viscosity modification purposes as a high resting viscosity is desirable to hold the structure at rest, and low flow viscosity is desirable during mixing.[2] Potential applications of CNF include cosmetics, personal care, pharmaceutical, paper and polymer composites.[2,17] CNF with hydrophilic coating has also been explored as reusable oil absorbents for oil spills.[18]

The objective of this study is to produce cost-efficient CNF comparable or exceeding the current commercial varieties. Rheological performance (shear thinning and storage/loss moduli) of produced CNF is the most important metric, since the potential application as a viscosity modifier is considered. A successful low-cost CNF production from a Bioconversion Network pulp can become a building block in the economic viability of biorefineries.

2. Literature review

2.1. Biomass feedstock

Biomass is composed of cellulose, lignin and hemicelluloses. [19] Cellulose has two common crystalline structures: cellulose I and II. Cellulose I is the stronger crystalline structure, which has more hydrogen bonding, and it is also the naturally occurring form.[15] Figure 2-1 shows the structure of cellulose I, where glucan chains run parallel and hydrogen bond in either I_α or I_β pattern. The difference between the two allomorphs is the slightly different positioning of glucan chains relative to each other, and the hydrogen bonding pattern is thus different. In higher plants such as trees, cellulose I_β is the dominant form and cellulose I_α only contributes to less than 20 %.[20] Although cellulose is the part of the lignocellulosic biomass that CNF is produced from, other components need to be noted as their presence can affect the production process. Lignin is a 3-dimensional polymer of phenylpropanes.[19] Since lignin gives mechanical support and its linkages are not hydrolyzable, it is tough to break down.[19] Hemicellulose consists of 25 – 30 % of dry wood, and it is a heteropolymer consisting of various pentose and hexose monosaccharides.[19] Due to its weaker mechanical properties, compared to cellulose, hemicellulose has not been explored as much as cellulose.[5] The biomass feedstock may also have trace amounts of ashes from burned biomass as well as sugars from hydrolyzed biomass, but they are not expected to have a large impact due to low concentration.

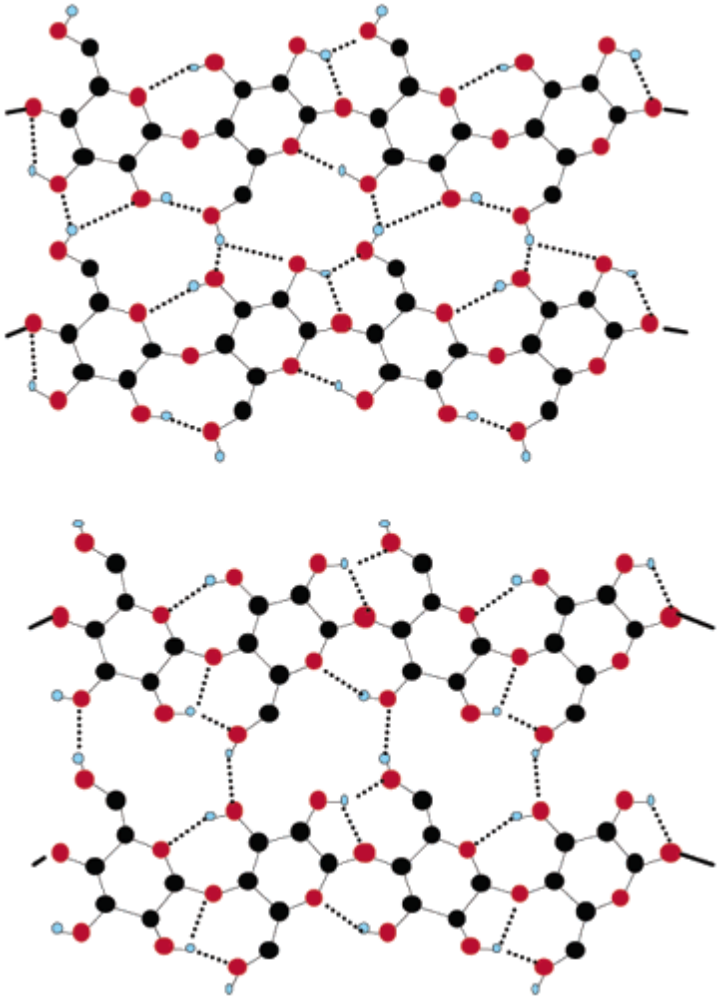

Figure 2-1 – Cellulose Iα (A) and cellulose Iβ (B) structures. (●) – C (●) - O, dotted lines represent hydrogen bonds.[21]

2.2. CNF production

There are several ways to produce CNF from lignocellulosic biomass: enzymatic, mechanical, carboxymethylation, TEMPO, weak acid hydrolysis and dissolution/electrospinning. Figure 2-2 is an overview of how frequently each method is used to produce CNF in literature, based on a SciFinder search by

Lavoine et al (weak acid hydrolysis and dissolution/electrospinning not included).[22]

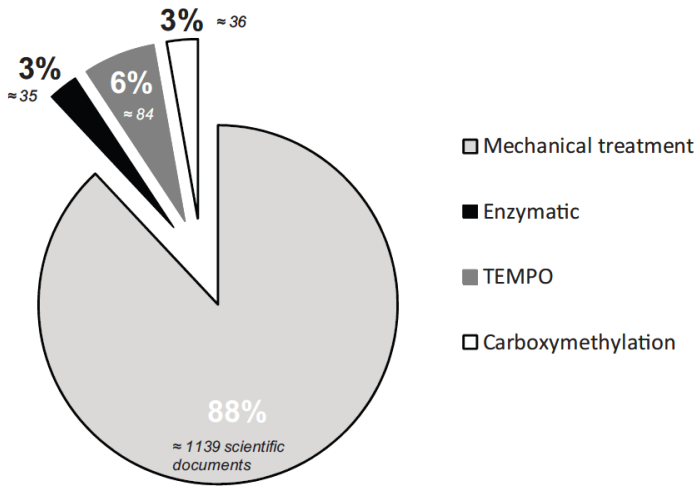

Figure 2-2 – Distribution of CNF pretreatments by literature search[22]

Mechanical treatment is the most popular production method according to Figure 2-2. Mechanical shearing is done by a microfluidizer, and it is a synthesis method that is highly commercializable with an industry scale microfluidizer. A pilot/production scale microfluidizer by Microfluidics is shown in Figure 2-3. Using a mechanical method means no chemicals or solvents other than water is needed for the synthesis, and no special handing is required. Another advantage is that microfluidizers do not require highly trained personnel for operation; a technologist can operate and do basic troubleshooting. However, a mechanical method often requires high energy input. One pass requires energy in the order of tens of kWh/tonne, and 14-30 passes are typically required to synthesize CNF.[16]

Figure 2-3 – Microfluidizer M-110EH-30 pilot/production process

Having such high energy inputs can damage the crystallinity and molecular weight of cellulose, resulting in inferior performing fibres.[2] The defibrillation occurs in chambers with narrow channels, and if a channel is blocked, it would lead to halting the production and clearing the chambers first.[16]

Enzymes can be used to break down cellulose fibres into CNF by attacking amorphous regions in cellulose bundles. Monocomponent endoglucase is an example of an enzyme that has been used to defibrillate cellulose.[16] The advantages are controlled reactions, selective targeting ensuring high aspect ratio and uniform distributions. However, a large hemicellulose content is needed to promote deaggregation, so that the enzymes can access the fibres. Enzymatic hydrolysis is also costly and slow.[16]

Carboxymethylation is a method that introduces charge into cellulose fibres and utilizes charge repulsion to delaminate.[2] A typical degree of substitution for carboxymethyl groups onto cellulose is 0.1.[2, 22] Figure 2-4 shows a carboxymethylation reaction of cellulose described by Eyholzer et al.

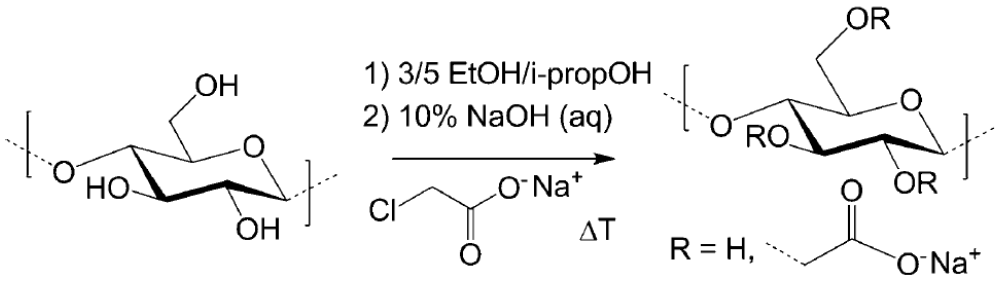

Figure 2-4 – Carboxymethylation reaction by chloroacetic acid[23]

An advantage of carboxymethylated CNF is that it can be redispersed after drying.[23] However, carboxymethylated CNF possess charges, thus the fibres repel each other reducing entanglement.[24]

The TEMPO (2,2,6,6-tetramethylpiperidine-1-oxyl) mediated oxidation creates CNF with surface charges by catalyzing oxidation of primary alcohol groups in cellulose.[2] In the TEMPO method reported by Saito et al, a slurry of pulp, NAClO, TEMPO and sodium bromide are reacted in basic pH up to 42 min. In order to achieve disintegration, the pulp must not be previously dried.[25] A simple mechanical treatment after TEMPO oxidation was needed to separate the cellulose microfibrils.[25]

Acid hydrolysis is frequently used to synthesize shorter (~100 nm) nanocelluloses.[2] In order to retain the length of glucan chains for CNF production, using a weak acid as opposed to a strong acid is necessary. For example, Abraham et al showed that including a 5 % oxalic acid step aids in defibrillation, but weak acid hydrolysis was not used exclusively for CNF synthesis.[26]

The dissolution and electrospinning method is different from other methods in that it is a bottom-up approach that synthesizes a weaker cellulose II morphology, thus not grouped with the other methods in Figure 2-2.[15] Fibres produced by electrospinning have diameters of 100 – 500 nm.[15] Cellulose is first dissolved in a solvent such as lithium chloride or N,N-dimethylacetamide. Figure 2-5 is a schematic of an electrospinning system where the fibres become suspended in a solvent in the coagulant bath. The wet cellulose filaments pumped by the micropump towards the tip of the injector, then they are sprayed onto a collector by electrostatic forces. Some important parameters that affect fibre size are suspension viscosity, surface tension and electrical field strength between injector and collector. The collector can be a solid such as aluminum, paper or a solvent such as water. [15] It is convenient to deposit films using electrospinning, since CNF can dry directly on the collector of choice.[27] The dissolution and electrospinning method produces larger diameter CNF with weaker cellulose II morphology.

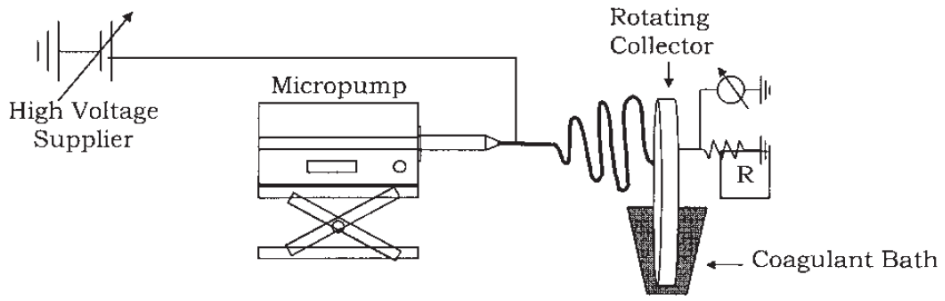

Figure 2-5 – Schematic of electrospinning system with coagulant bath[15]

The CNF production methods described above can be combined to produce CNF more efficiently. For example, enzymes and mechanical shearing have been combined to yield high aspect ratio CNFs by Pääkkö et al.[16] There has also been development on combining mild chemical treatments and mechanical treatments, which resulted in 15-25 nm diameter fibres.[26]

2.3. CNF morphology

CNF morphology have been characterized by imaging techniques such as atomic force microscopy, scanning electron microscopy and cryo-transmission electron microscopy (cryo-TEM).[15-16] Scanning electron microscopy uses electron beams to image the sample up to about 30 kV, and it is capable of achieving nanometer resolution. Figure 2-6 is a simplified schematic of a scanning electron microscope in transmission mode.

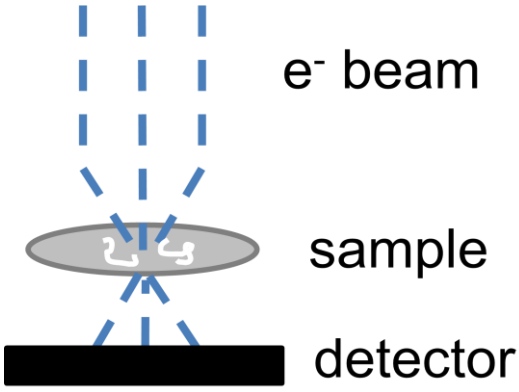

Figure 2-6 – Simplified schematic of scanning transmission electron microscope

Polymers such as cellulose are susceptible to electron beam damage.[28] Cellulose is fairly resistant to temperature effects compared to other polymers, but its carbon backbone can still be damaged with electron beams above the acceleration voltage of 86 kV. Thus imaging should be conducted at a lower voltage, unless beam damage can be mitigated by other means.[29] Since CNF is a biopolymer consisting of light elements that do not absorb electrons well, it is important to increase image contrast to improve image quality. Contrast can be improved with stains such as uranyl acetate.[30] TEM the highest resolution technique used on CNFs. Since CNF is a can be damaged by high energy electrons in TEM, performing TEM in cryogenic conditions is necessary.[16] For example, Pääkkö et al imaged CNF at -180 °C and 120 kV acceleration voltage.[16] Atomic force

microscopy has also been used to image CNF in tapping mode with silicon cantilevers.[16]

Dynamic light scattering (DLS) is also known as photon correlation spectroscopy (PCS) and quasielastic light scattering (QELS). DLS is a particle characterization method that uses a laser beam to determine the diffusion coefficient, and thus the hydrodynamic diameter. This method is most accurate for spherical particles, but fibre lengths can be approximated as Brownian rods.[25]

In DLS, a laser beam is shined onto the sample vial, and the scattering is monitored at a certain angle. The scattered laser beam is used to determine intensity of the autocorrelation function shown in Equation (2-1),

$$G^{(2)}(\tau) = A[1 + \beta\left|g^{(1)}(\tau)\right|^2] \qquad \textbf{(2-1)}$$

where τ is the delay time, A is the baseline, β is the spatial coherence factor and $g^{(1)}$ is the first order normalized electric field correlation function.[31] Equation (2-2) is an expression of $g^{(1)}$,

$$g^{(1)}(\tau) = G(\Gamma)\exp(-\Gamma\tau)\,d\Gamma \qquad \textbf{(2-2)}$$

where Γ is the average linewidth, G(Γ) is the normalized characteristic linewidth distribution function.[31] Integrating Equation (2-2) with respect to Γ as particle concentration approaches 0, Γ can be expressed as Equation (2-3),

$$\Gamma = D_t q^2 \qquad \textbf{(2-3)}$$

where D_t is the translational diffusion coefficient and q is the magnitude of momentum transferring vector.[31] For spherical particles, the hydrodynamic diameter d_h can be expressed as Equation (2-4),

$$d_h = \frac{k_B T}{3\pi\eta_o D_t} \qquad \textbf{(2-4)}$$

where k_B is Boltzmann's constant, T is temperature and η_o is the viscosity. [31] The translational diffusion constant D_t relates to length and diameter for Brownian rods as expressed in Equation (2-5).[25]

$$D_t = \frac{k_B T}{3\pi\eta_o L}\left[ln\left(\frac{L}{d}\right) + 0.312 + 0.565\frac{d}{L} + 0.100\left(\frac{d}{L}\right)^2\right] \qquad \textbf{(2-5)}$$

As equation (2-3) only applies when concentration approaches 0, the accuracy of DLS is affected by the suspension concentration. The concentration regimes are shown in Figure 2-7. In the dilute regime, the CNF fibres do not touch each other, thus they can move freely. When a suspension enters the semi-dilute regime, the hydrodynamic volume of CNF fibres touch and movement is hindered.[32]

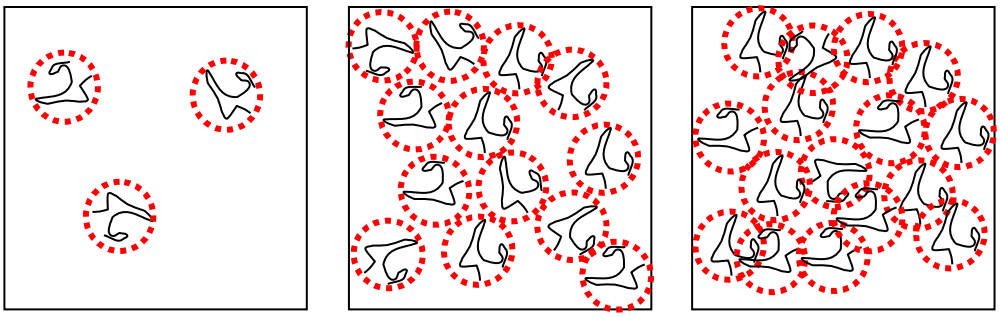

Figure 2-7 – Diagrams of dilute, semi-dilute and concentrated suspension regimes

Since DLS measures the translational diffusion coefficient, the particles must be in dilute regime. To calculate the critical concentration c* between dilute and semi-dilute regime of CNF, a rigid rod approximation can be used. Equation (2-6) shows that c* in vol % is dependent on fibre diameter (d) and length (L).[33]

$$c^* = \frac{d^2 L}{L^3} \qquad \textbf{(2-6)}$$

2.4. CNF Colloidal stability

An important desirable property for commercial formulations such as cosmetics and pharmaceutical products is stability.[32] The stability of CNF has been measured by dynamic light scattering (DLS) as a semi-quantitative method.[34] Gel formation was studied by Fall et al with DLS over time to characterize the difference in fluctuations, but the same method can be used for studying settling.[34]

Turbiscan turbidity meter is another instrument has been used to characterize suspension stability.[35] Instead of a fixed laser height in DLS, Turbiscan scans the sample vial from bottom to top for a more comprehensive settling profile. A schematic of Turbiscan is shown in Figure 2-8. As the laser scans the sample vial, part of the beam is backscattered, part of it is transmitted. The change in transmission and backscattering data corresponds to the change in the number of particles in the laser's path.

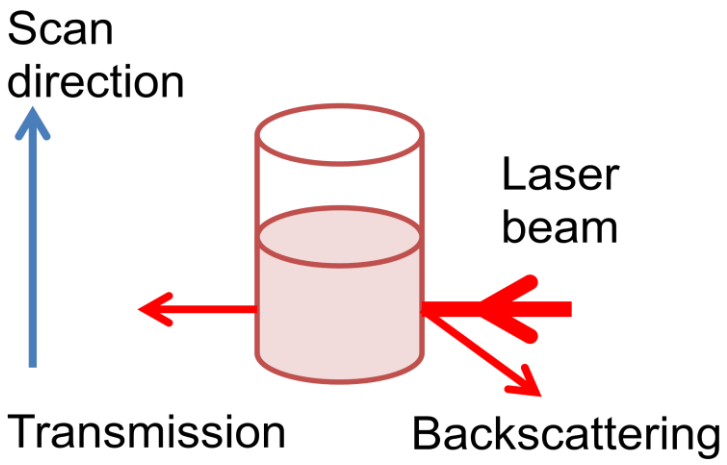

Figure 2-8 – Simplified schematic of a turbidity meter

2.5. Small amplitude oscillatory shear

Small amplitude oscillatory shear rheology can be used for mechanical properties such as storage (G') and loss moduli (G") by oscillating a probe on the sample suspension at various frequencies. In ideal gels, the G' and G" are independent of angular frequency and G' >> G". Polymer gels are traditionally crosslinked

polymers, but CNFs form an entangled network with physical crosslinking, which constitute as a pseudo-gel.[36] In Figure 2-9, the G' and G'' of CNF are presented.

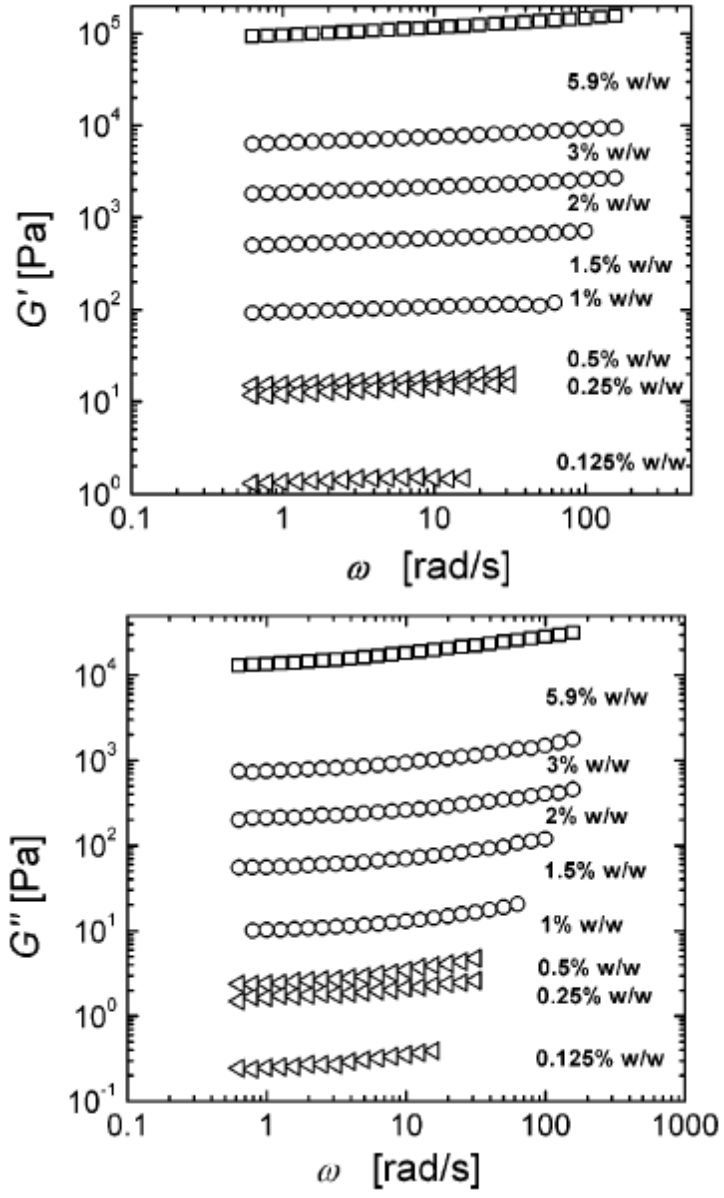

Figure 2-9 – CNF G' and G'' by Pääkkö et al[16]

In crosslinked polymer gels, G' > G" up to the critical gel point after which G' > G" and the moduli become independent of stress/strain, forming a gel.[36] According to the behaviour of G' and G" in Figure 2-9, CNFs behave like gels from 0.5 to above 10 rad/s oscillation frequency, and there is no critical gel point. At higher frequencies (approximately >100), the gel begins to break down. Concentration of CNF is positively correlated to gel breakdown frequency, thus higher concentration CNF can maintain gel behavior for higher frequencies.

2.6. Steady state shear

The viscosity of CNF decreases with increasing shear rate, a phenomenon known as shear thinning.[16] Figure 2-10 shows the viscous behaviour of a CNF from 0.25 to 5.9 wt %. Shear thinning occurs over a wide range of shear rate from 0.1 to 1000 1/s. The viscosities are proportional to CNF concentration, since higher concentration CNF suspensions have higher entanglement, leading to higher viscosity.[37] The shear thinning behaviour of CNFs can be explained by the alignment of fibres when shear force is applied, thus decreasing the viscosity.[37] Due to high entanglement of CNF, it does not quickly break down to a low viscosity suspension with applied shear force.[16]

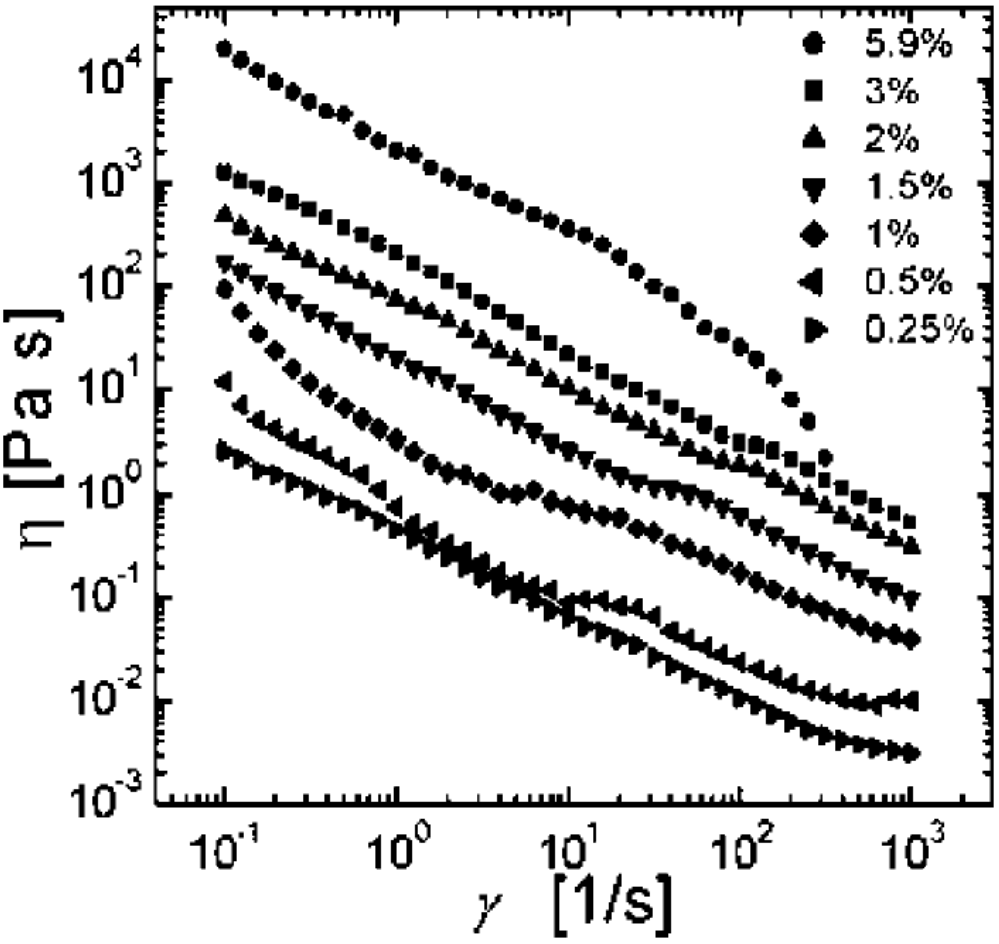

Figure 2-10 – CNF viscosity vs. shear rate at 0.25 – 5.9 wt % by Pääkkö et al[16]

2.7. Salt effect

Adding salt will reduce the electrostatic repulsion between fibres, and CNF suspension will increase in viscosity according to a study by Fall et al.[24] The CNF used in Fall's study was produced by carboxymethylation induced swelling, thus they possess charges. The salt effect is not expected to align completely for CNF that do not possess charges, such as mechanically treated CNF. In general, higher

electrostatic repulsion is inversely proportional to viscosity of CNF suspensions, because electrostatic repulsion affects fibre interaction.[16]

3. Material and methods

3.1. Materials

3.1.1 Commercial CNFs

Two CNFs were used for this study. CNF A is an industrial grade product from Daicel Fine Chemicals, with product code KY100G. According to manufacturer, the solid content of KY100G is 10.6 wt % in water, and it appears to be a white, cotton-like semi-solid. The manufacturer provided information on CNFA with length between 0.4-0.5 mm and diameter between 0.01 μm – several μm. CNF B is a semi-commercial product from Innventia AB. It has a 2.5 wt % solid content and appears as a thick, white fluid. The CNFs were stored at 4 °C.

3.1.2 CNF feedstock pulps

CNF was produced from two pretreated biomasses, which were taken from the biorefining process line: 1) Organosolv pretreated soft wood (OP) from UBC; 2) Steam exploded and partially enzymatically hydrolyzed soft hardwood (MP) from Mascoma.

Lodgepole pine trees infested by mountain pine beetle at the gray phase were harvested at Prince George, and Quesnel BC, Canada, which were used as a feedstock for OP. The average age of the trees was 99 years as described by Pan et al.[38] After being debarked and air-dried, the tree trunks were chipped and

screened using a plate screen; the fraction with a size between 2.5x2.5 cm and 5.0x5.0 cm and approximately 0.5 cm thick was collected as the feedstock for ethanol organosolv pretreatment.

The lodgepole pine chips were pulped in a 65% solution of aqueous ethanol with 1.1% sulfuric acid as a catalyst (weight on wood chips) at a liquor to wood ratio of 7:1. The pulping was performed using a custom-built, four-vessel (2 L each) rotating digester (Aurora Products Ltd., Savona, BC, Canada). Four 200 g (oven dried weight) batches of chips were pulped in each of the four vessels. Vessels were opened after being cooled to room temperature in a water bath. The pretreated chip samples were pooled and washed together with a fresh solution of 65% ethanol preheated to 60 °C as described previously.[38] The sample was subsequently washed with water that was preheated to 60 °C. The washed substrate was split into 8 equal portions and homogenized in a standard British disintegrator for 5 min and passed through a laboratory flat screen with 0.008 in (0.203-mm) slits (Voith, Inc., Appleton, WI). The amount of rejects collected after screening the pulp was 4.2% of the starting feedstock. After pulping, in order to preserve the carbohydrates in the pulp, the sample was delignified at room temperature using acidified sodium chlorite according to PAPTAC method G10.U. The chemical composition of the resulting delignified organosolv pulp was measured according to the method outlined by Sluiter et al.[39]

The pulp received from Mascoma is wood that went through steam explosion and partial enzymatic hydrolysis, known as mechanical pulp or MP. This pulp is the leftover biomass from the enzymatic hydrolysis step, thus considered a waste product. Further details of the pulping process were unavailable due to the proprietary nature of the research. Table 3-1 shows the compositional analysis of both pulps.

Table 3-1 – Compositional analysis of OP and MP

	OP	MP
Cellulose	93 %	40 %
Hemicellulose	-	3.5 %
Lignin	2 %	57 %
Ash	-	0.5 %
Sugars	3 %	-

From Table 3-1, the cellulose percentage is very high in OP, and less than 50 % in MP, which is expected as OP went through delignification. A 57 wt % of lignin in MP is expected to be difficult to process, as lignin does not break down easily.

3.2. Conversion to CNF

Two types of pulp were suspended in water at 1 and 0.5 wt %. The RC suspension was chopped with a high shear mixer for 10 min/500 mL suspension. Organosolv pretreated pulp particle size was too large and clogged the high shear mixer mesh,

therefore it was first chopped by a Black & Decker Cyclone kitchen blender at speed 18 for 6 min. Then OP was high shear mixed for 10 min/500 mL suspension.

The fibrillation of chopped pulp was done by multiple passes through the microfluidizer (Microfluidics M-110EH-30). The chambers used were z-shaped, with 3 different chamber diameters: 200 µm, 100 µm and 87 µm. There was also a chamber referred to as "blank", which has wide mm range diameter. The blank chamber was not narrow enough to fibrillate cellulose, but it was used as a place holder as two chambers are required for microfluidizer operation. A diagram of a z-chamber used in the microfluidizer is shown in Figure 3-1, where the hollow arrows indicate the flow of pulp.

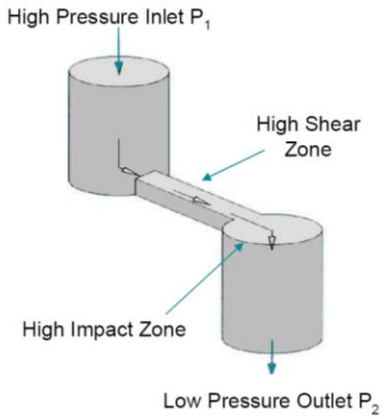

Figure 3-1 – Microfluidizer z-chamber diagram [40]

As seen in Figure 3-1, the pulp is pushed through a chamber by high pressure, and defibrillation occurs at the narrow high shear zone in the middle. In the two

chamber configuration in M-110EH-30 microfluidizer, the first chamber should always have a larger chamber diameter than the second one. When the second chamber is larger, the fibre output from the first chamber is already small and the second chamber will not serve a significant function.

If the pulp size is too large or does not defibrillate in the chamber, it may clog the chamber. Once a chamber is clogged, it needs to be flushed in reverse, and the process has to be restarted. On the other hand, a larger chamber does not fibrillate as efficiently as a smaller one, thus optimum chamber sizes must be found for each microfluidizer pass. The prepared CNF suspensions were stored at -4° C.

3.3. Characterization

3.3.1 Scanning electron microscopy

A Hitachi S4800 scanning electron microscope was used to image CNFs in transmission mode. A low concentration (0.1 - 0.01 wt %) aqueous CNF suspension droplet was applied on carbon copper grid and allowed to rest for 2 min. The droplet was blotted with filter paper and allowed to dry for 2 min. Since cellulose is composed of low molecular weight atoms, the sample was stained to improve contrast. 2 wt % uranyl acetate stain was prepared by dissolving solid uranyl acetate in nanopure water by sonication, and the solution was filtered to ensure not solid particles would interfere with imaging. One drop of the stain was applied on the sample grid and after 5 min it was blotted with filter paper. The

stained sample grid was allowed to dry for 10 min, and then stored in a desiccator to prevent moisture deposition. Sample grid preparation was done a day or two before STEM analysis, as longer storage may lead to degradation and contamination. STEM was conducted at room temperature using an acceleration voltage of 30 kV and emission current of 20 µA. The instrument is capable of 0.5 – 30 kV accelerating voltage, and the highest voltage was chosen due to higher resolution. Electron beams at 30 kV are not expected to break cellulose bonds at room temperature.

3.3.2 Dynamic light scattering

Dynamic light scattering (DLS) was used to determine the hydrodynamic radius of CNF particles. The DLS was a Malvern Zetasizer Nano-Swith a 4.0 mW He-Ne laser at 633 nm and an Avalanche photodiode detector. The instrument was working at 173° scattering angle. It was conducted with 0.1 wt % CNF suspension in water. Disposable 1 cm pathlength cuvettes were used. The size distribution was calculated using an inverse Laplace transform algorithm, and the fibre length was calculated using Equation (2-5) in section 2.3. Measurements were obtained with a temperature regulated cell set at 25 ± 0.1 °C. The same sample was tested three times consecutively.

3.3.3 Charge measurement

Charge measurements were taken with a Thermo Scientific DuraProbe 4-electrode graphite electrode for Orion5 Star PlusMultimeter. The cell was calibrated with 1413 µS/cm standard, which was the lower concentration standard that was part of the electrode kit. The standard was chosen because the native CNF salt concentration was expected to be very low due to the production processes and manufacturer specifications. Measurements were conducted at room temperature.

3.3.4 Preparation of suspensions

CNF suspensions at 0.125, 0.5 and 0.75 wt % were prepared for rheological studies. Since the CNF suspensions used for rheology have very dilute concentrations, they are suspended in 1:1 ethylene glycol:water by weight for a higher background viscosity. The ethylene glycol used was from solution grade from Sigma Aldrich, and the water used was nanopure water from Thermo Scientific™ Barnstead Nanopure ultrapure water purification system. The suspensions were prepared by adding concentrated aqueous CNF stock to a glass vial, then adding ethylene glycol and water to make up 1:1 weight ratio. All added materials were measured by a balance. The suspensions were vortex mixed and stirred with a magnetic stirrer for at least 5 hours to ensure the fibres are well suspended.

CNF suspensions with NaCl salt at 10 mM, 25 mM, 50 mM and 100 mM were also prepared from CNF A. The preparing method with added salt is the same as described above, except instead of adding water, a combination of 250 mM NaCl and water was added to make up the appropriate salt concentration from 10-100 mM.

3.3.5 Colloidal Stability

The stability of CNF suspensions were measured with a Formulation Smart Scientific Turbiscan instrument. Turbiscan scans the sample vial from bottom to top and measures the transmission and backscattering. CNFs were suspended in 1:1 ethylene glycol:water at 0.125 wt % for Turbiscan measurements. Before the suspensions were put in Turbiscan vials, they were inverted several times for a uniform fibre distribution. The suspensions were inserted glass Turbiscan vials by a glass pipette up to about 12 mm. Care was given to not contaminate the side walls of the glass vial with fluid above the meniscus, and the vial was not tilted to ensure a clean meniscus could be read by the Turbiscan machine. Each sample was scanned once per minute for 1 hour.

3.3.6 Small amplitude oscillatory shear

Dynamic rheology of CNFs was measured by an AR G2, TA instruments rheometer. A cone-and-plate geometry was used, which allows for low sample volume and accurate rotation generation. The cone was a 60 mm aluminum cone

with 1° angle, and it is suitable for low to medium viscosity fluids. The gap was set at 56 µm. The samples were inverted three times to mix, and allowed to rest for 5 min before each measurement to ensure the chains are relaxed. The measurements were taken at 25 °C. To determine the linear viscoelastic range, torque sweep was measured for 0.01 – 100 Pa at 1 Hz. The strain of 0.07 was chosen for the CNF suspensions for frequency sweeps 0.01 – 100 Hz.

3.3.7 Steady state rheology

Steady state rheology of CNFs was measured with the same geometry, cone and settings as steady state rheology. Viscosity of CNF suspensions were measured against shear rates from 0.1 – 100 1/s.

4. Results and Discussions

4.1. CNF production

MP worked well at 0.5 and 1 wt %, but OP clogged the homogenizer at 1 wt %. Even at 0.5 wt % OP, the pulp required going through a blender before using the homogenizer. Table 4-1 and Table 4-2 show the optimal microfluidizer chamber sizes for the two pulps.

Table 4-1 – CNF MP Production Microfluidizer Chamber Sizes

Pass #	1st Chamber Size	2nd Chamber Size	Pressure (MPa)
1	Blank	200 µm	21
2	200 µm	100 µm	34
3	200 µm	100 µm	34
4	200 µm	87 µm	41
5	200 µm	87 µm	41
6	200 µm	87 µm	41
7	200 µm	87 µm	41

Table 4-2 – CNF OP Production Microfluidizer Chamber Sizes

Pass #	1st Chamber Size	2nd Chamber Size	Pressure (MPa)
1	Blank	200 µm	21
2	Blank	200 µm	21
3	Blank	200 µm	21
4	Blank	200 µm	21

From the microfibrillation results, MP fits through smaller chamber sizes, which implies MP has smaller particle size than OP. CNF MP was put through more passes through the microfluidizer than CNF OP because subsequent characterization results show CNF OP to have acceptable fibrillation and performance at fewer passes. The energy consumption and estimated prices are presented in Table 4-3 based on Table 4-1 and Table 4-2.

Table 4-3 – Energy consumption of CNF MP, OP and B

	CNF MP (Microfluidizer)	CNF OP (Microfluidizer)	CNF B (whole process)
Energy input (kWh/kg)	500	300	600[41]
Cost (CAD/kg)	5	3	6

The energy price is set at 1c/kWh, based on average pricing from the Alberta's Utilities Consumer Advocate.[42] CNF OP production requires much less energy compared to CNF MP, therefore it is more cost-efficient. The energy consumption of produced CNF is in the same range as CNF B, but they do not include energy from pretreatment processes. However, the production was done at pilot/lab scale, and further scale-up is expected to lower energy consumption per kilogram. In conclusion, the estimated CNF energy consumption is comparable to commercial CNF and it has potential of being cost-efficiently scaled up.

A photograph of CNF MP produced from 7 microfluidizer passes is shown in Figure 4-1.

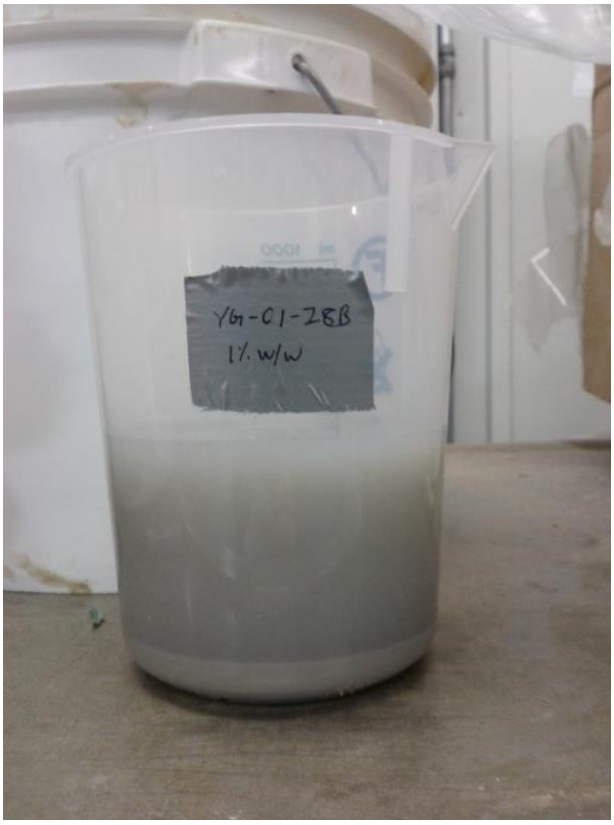

Figure 4-1 – Photograph of CNF MP suspension

CNF MP appears as a brownish grey suspension that is relatively opaque. The top appears more transparent as settling of the fibres occurred, and there is a dense layer of cake in the bottom. A photograph of CNF OP produced from 4 microfluidizer passes is shown in Figure 4-2.

Figure 4-2 – Photograph of CNF OP suspension

CNF OP is a white suspension that is semi-opaque, and it appears similar to commercial varieties. There is some visible settling as the top appears more transparent, but no dense cake forms in the bottom. Based on physical appearance, CNF OP is superior since it has a more appealing white colour that commercial CNFs also possess, and it does not form a cake like CNF MP.

4.2. Scanning electron microscopy

Some typical scanning electron micrographs of CNF A/B, MP and OP are shown in Figure 4-3, Figure 4-4 and Figure 4-5 respectively.

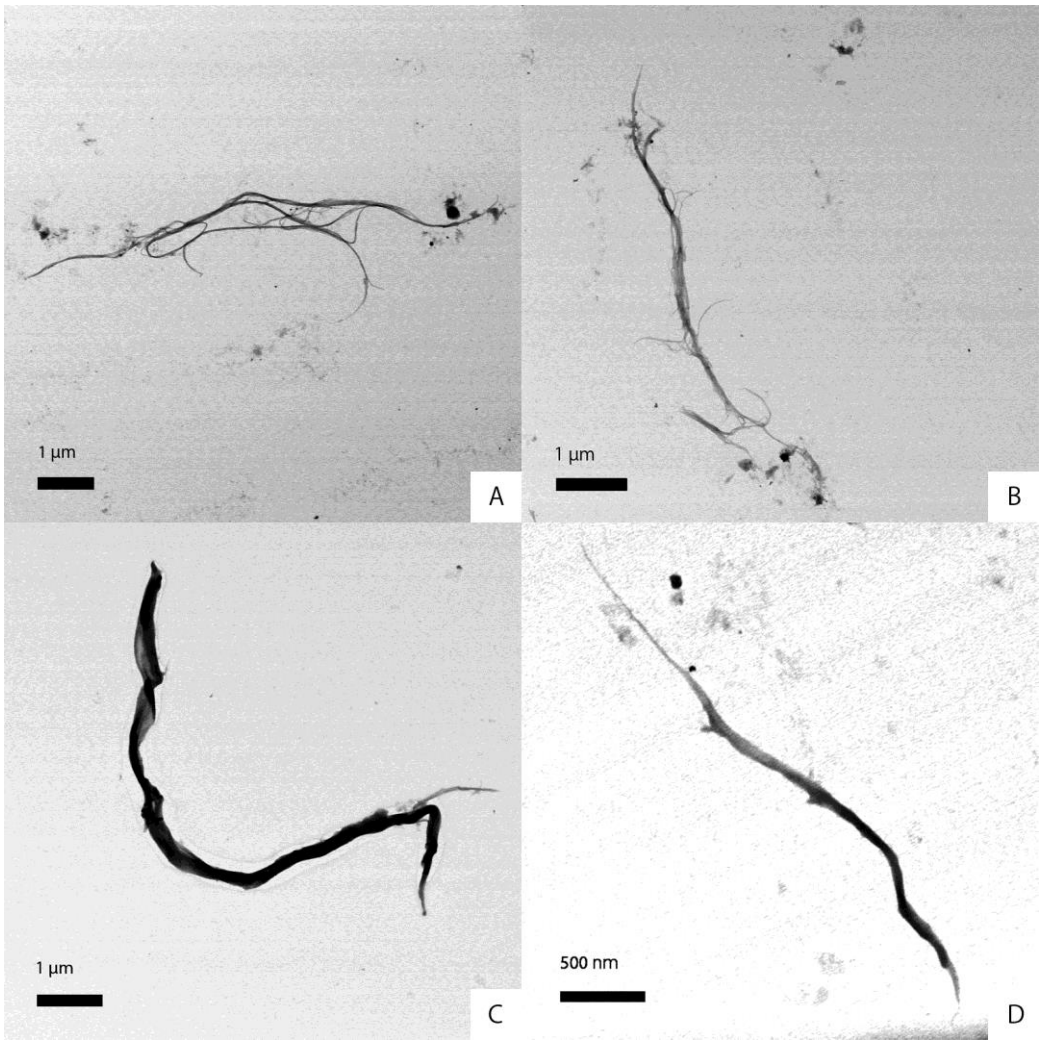

Figure 4-3 – STEM Micrographs of CNF A (A,B) and CNF B (C,D)

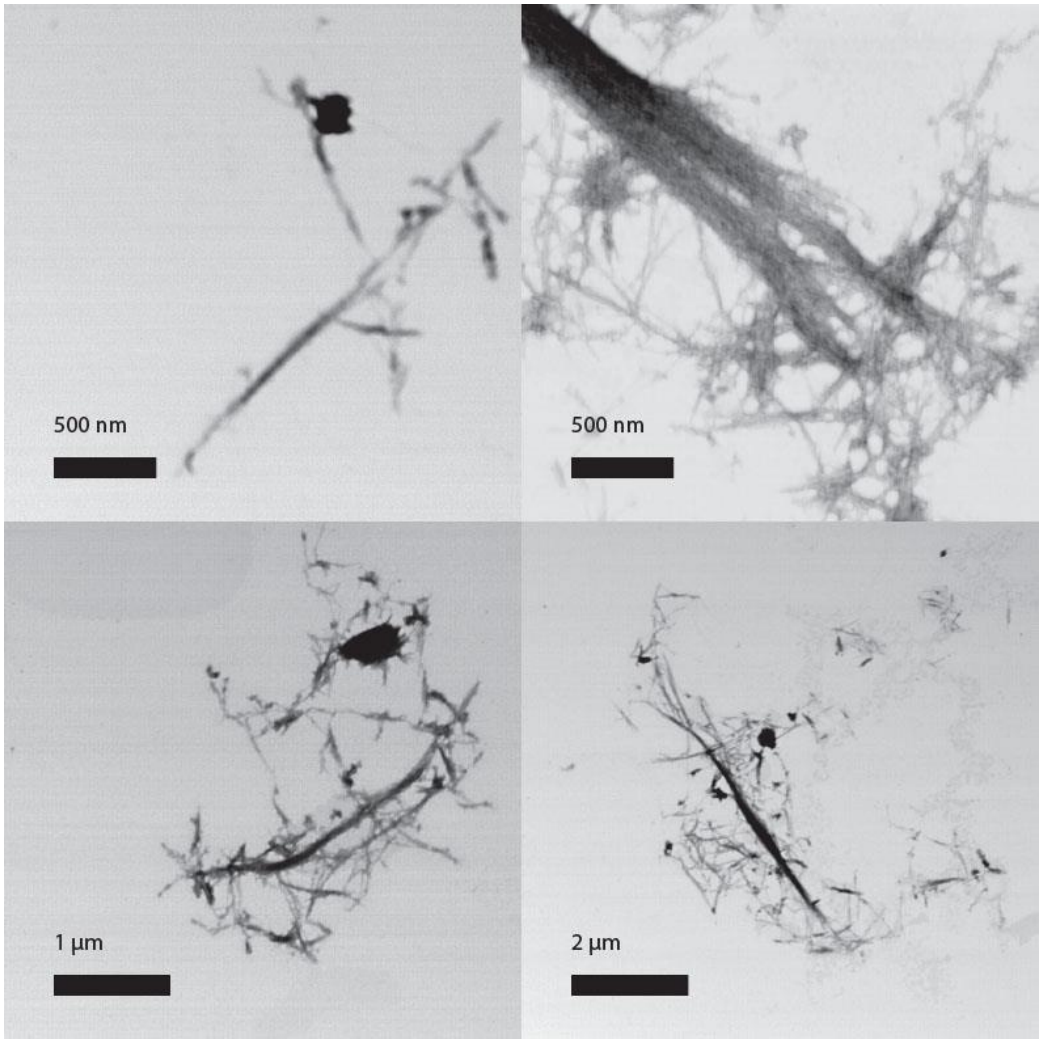

Figure 4-4 – CNF MP STEM Micrographs

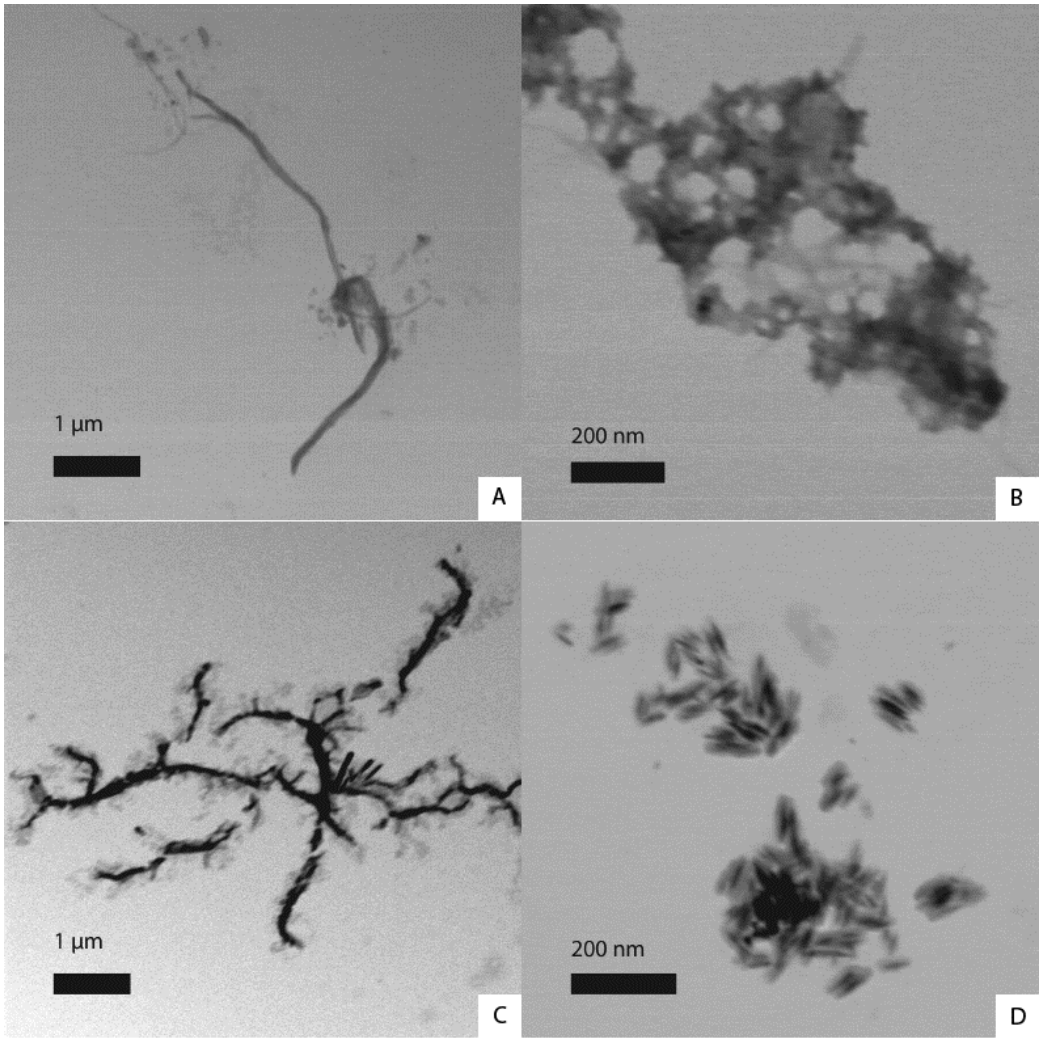

Figure 4-5 – CNF OP STEM Micrographs

The diameters of the CNFs were measured from a total of 33 STEM micrographs, and the averages are presented in Table 4-4.

Table 4-4 – Average CNF diameters by STEM

CNF Type	Average Diameter (nm)
A	98
B	180
MP	345
OP	42

From Figure 4-3, the commercial samples CNF A and B are linear with some defibrillated side chains, which is in agreement with literature and manufacturer specifications in section 3.1.[16] CNF A has smaller diameter and it is longer than CNF B from scanning electron micrographs, and CNF A is more fibrillated and loose. Thinner fibres are have more fibres per gram and they are able to form entangled networks at lower concentrations, thus CNF A is expected to have higher viscosity performance at low concentrations based on STEM. On the other hand, CNF B appears more thick and rigid, which might result in jamming. CNF MP micrographs in Figure 4-4 show some finely fibrillated thin fibres with more branching than commercial CNFs, but also poorly defibrillated portions. In Figure 4-5, CNF OP has fibrous, porous, star-branched and cellulose nanocrystalline structures. Although the particle sizes are larger than the commercial CNFs, the structures observed have high surface area.

Additionally, CNF A has an average length of 6.7 µm, which fall into the range of manufacturer specifications as described in section 2.1. CNF B's average length was found to be 5.9 µm. The average length of CNF MP was difficult to determine from STEM micrographs as many exceeded the size of the micrographs. CNF OP had different morphologies, and length could not be defined.

4.3. Overlap concentration

The overlap concentrations of CNFs were calculated by Equation 2-6, and presented in Table 4-5. The weight percent overlap concentrations were obtained from the volume percent by diving with the density of cellulose (1.5 g/cm^3) with the assumption that cellulose weight is negligible compared to solvent weight.

Table 4-5 – Overlap concentrations of CNF A and B

CNF	Length (nm)	diameter (nm)	c* (vol %)	c* (wt %)
A	6700	98	0.021%	0.032%
B	5900	180	0.093%	0.140%

The overlap concentration of CNF A is lower than CNF B due to its higher aspect ratio and thinner diameter. DLS results are expected to be accurate when the concentration is < 0.032 wt % for CNF A and < 0.140 wt % for CNF B. Since the CNF fibres are not touching below the overlap concentration, a 3-dimentional entangled network cannot form, which would lower the suspension's rheological

performance. The overlap concentration for CNF MP was not calculated due to lack of data for CNF length by STEM. The overlap concentration for CNF OP was not calculated due to the difficulty in determining length with its complex morphology, and the rigid rod approximation in Equation (2-5) would be far from the actual morphology of CNF OP.

4.4. Dynamic light scattering

The effective diameters of CNF A and B from DLS fall into the expected length range. The DLS relative intensity and effective particle diameter of CNF A and BMP are presented in Figure 4-6 and Figure 4-7.

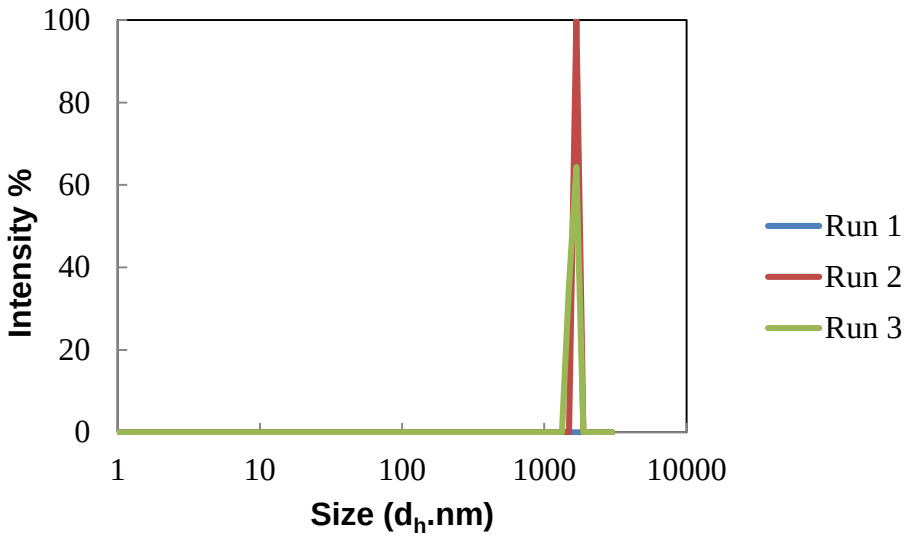

Figure 4-6 – DLS size distribution by intensity of CNF A

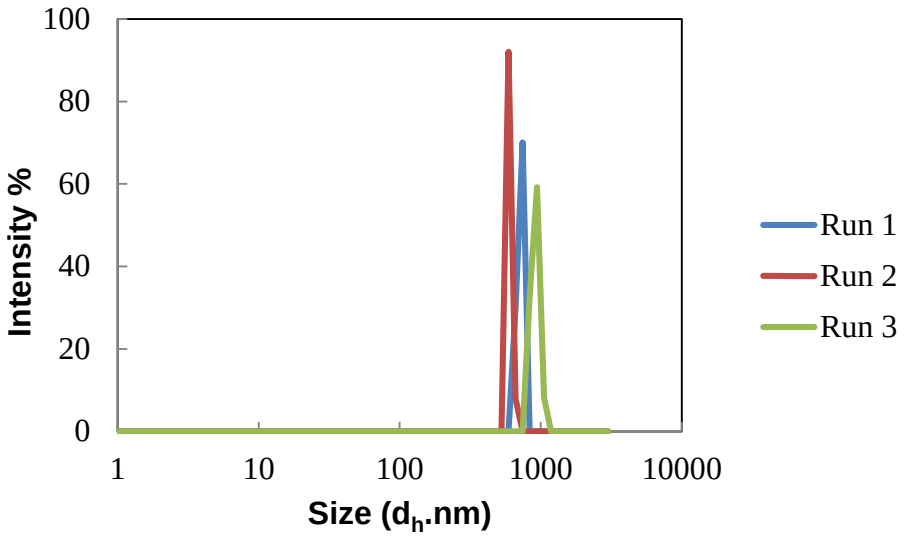

Figure 4-7 – DLS size distribution by intensity of CNF B

Since CNF MP sedimented readily to form cake in the bottom, two DLS analyses were made on it. The top layer DLS results are shown in Figure 4-8, and the whole analysis including the cake is shown in Figure 4-9.

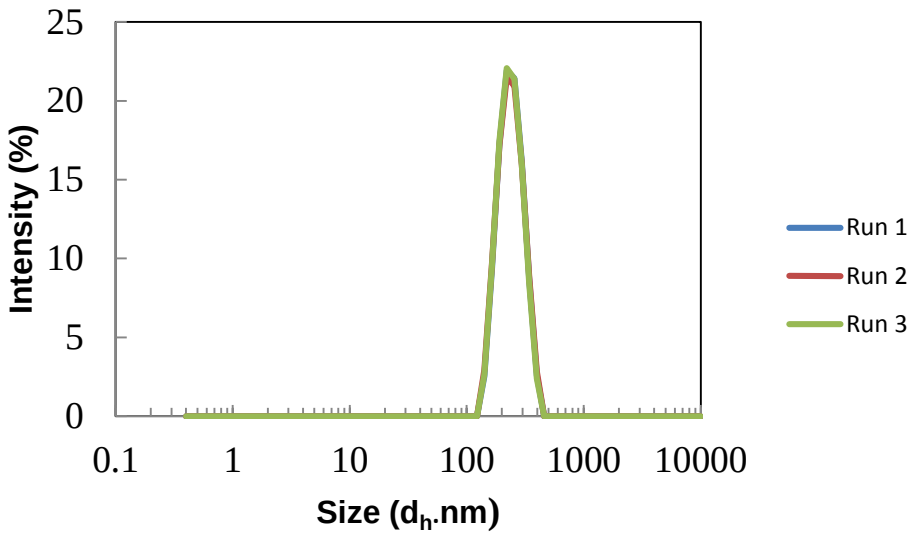

Figure 4-8 – DLS size distribution by intensity of CNF MP (top)

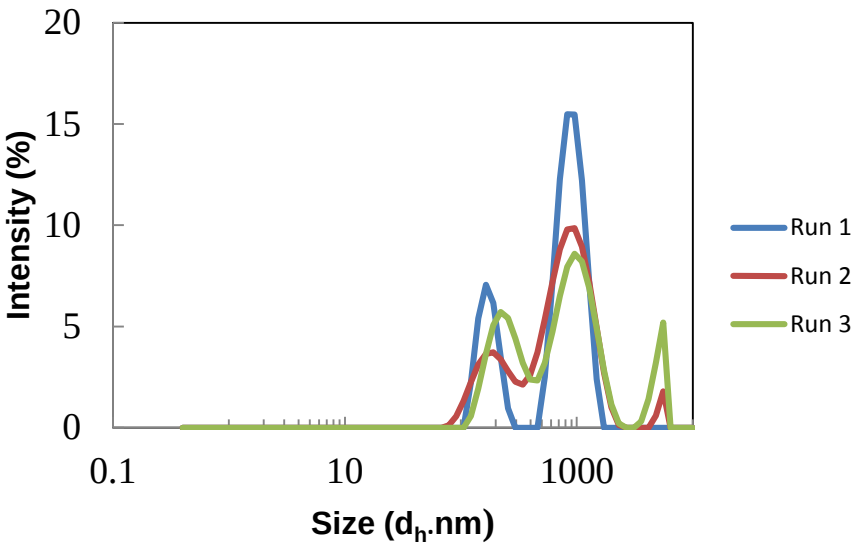

Figure 4-9– DLS size distribution by intensity of CNF MP (whole)

Table 4-6 presents the hydrodynamic diameter and calculated lengths based on diameters obtained from STEM (Table 4-4) and diffusion constants from DLS by Equation (2-5).

Table 4-6 – DLS results of CNF fibres

	CNF A	CNF B	CNF MP (top)	CNF MP (whole)
d_h (nm)	1647±46	766±161	594±104	N/A
Length (µm)	7.7	2.1	N/A	N/A
Shape factor	77	12	N/A	N/A

Comparing Table 4-6 and Table 4-4 from STEM, the lengths for CNF A are close at 7.1 µm by DLS and 6.7 µm by STEM. CNF B has a larger deviation at 2.1 µm by DLS and 5.9 µm by STEM. The concentrations used for DLS were 0.1 wt %, and it is higher than the overlap concentration calculated for CNF A in section 4.3, which can result in inaccurate results. CNF MP (top) showed one peak similar to commercial varieties with a smaller size. The whole CNF MP analysis had three peaks, indicating high polydispersity in the fibres. The DLS results of CNF MP are in agreement with STEM results, since it shows large particles as well as smaller ones. The top layer results are the proper CNF fibres that were liberated from lignin, thus defibrillated into CNF. The bottom cake should have high lignin content, since it does not break down readily, resulting in large particle sizes. The difference between the DLS and STEM results can be attributed to the following reasons: DLS is a macroscopic method and STEM is a microscopic method that examines individual fibres, DLS is conducted in solution and STEM sample is dried, Equation (2-5) is an approximation for rigid rods, whereas CNF is flexible and branched.

4.5. Conductivity

Table 4-7 shows the conductivity measurements of CNF A, B, MP and OP with and without added salt.

Table 4-7 – Conductivity measurements of CNFs at 0.2 wt %

CNF Type	NaCl Added (mM)	Conductivity (µS/cm)
A	0	3.4
A	10	412
A	25	959
A	50	1864
B	0	1.5
MP	0	4.2
OP	0	7.9

All CNFs show very low conductivity (<10 µS/cm) without added salt, and the ionic concentrations are insignificant compared to the conductivity of samples with added NaCl. The low conductivity of CNF suspensions without added salt indicates that electroviscous effects can be ignored for unsalted suspensions.

4.6. Colloidal stability

The backscattering and transmission data obtained by Turbiscan are shown in Figure 4-10 to Figure 4-13. As the fibers settle, backscattering will increase in the bottom of the vial and transmission will increase on top. Vials were filled up to about 14 mm. The top of the suspension is characterized by a peak in transmission in referenced mode, and a sharp increase in transmission in no reference mode. CNF MP backscattering at the bottom of the suspension increased 5% in 1 h, and

such steep increase indicates quick sedimentation. CNF OP, A and B backscattering only showed less than 1 % change, which indicate lack of sedimentation. The transmission on top decreased for all CNF, and the order starting from least change to most change is CNF A, CNF MP, CNF OP, CNF B. In summary, all suspensions showed settling over 1 h, but CNF MP showed sedimentation in the bottom while other CNF did not.

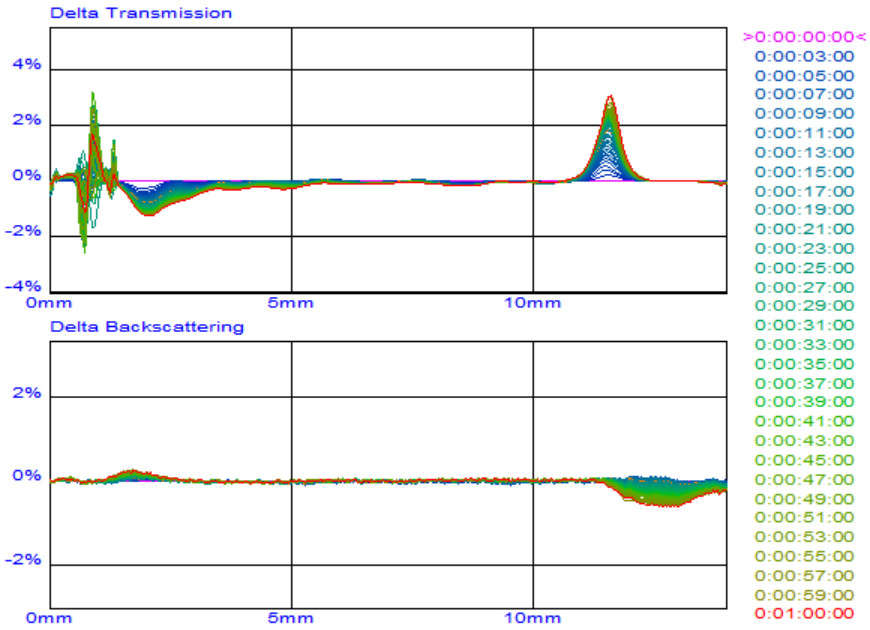

Figure 4-10 – Turbiscan Results of Commercial CNF A

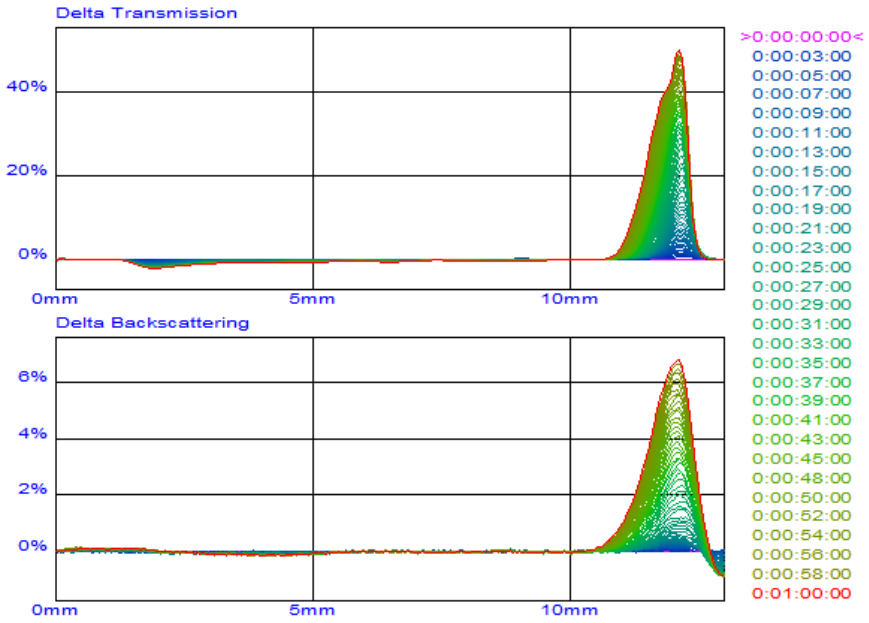

Figure 4-11 – Turbiscan Results of Commercial CNF B

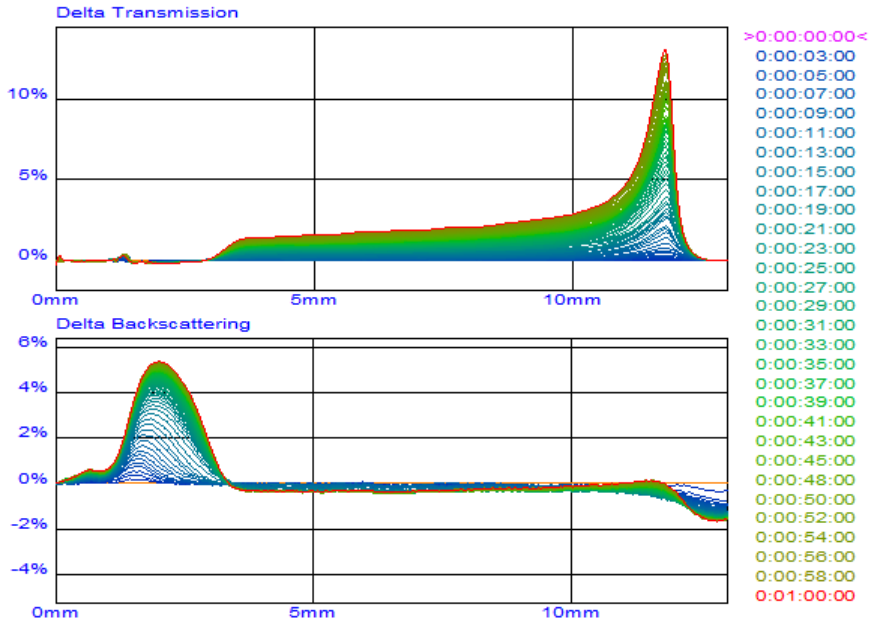

Figure 4-12 – Turbiscsan Results CNF MP

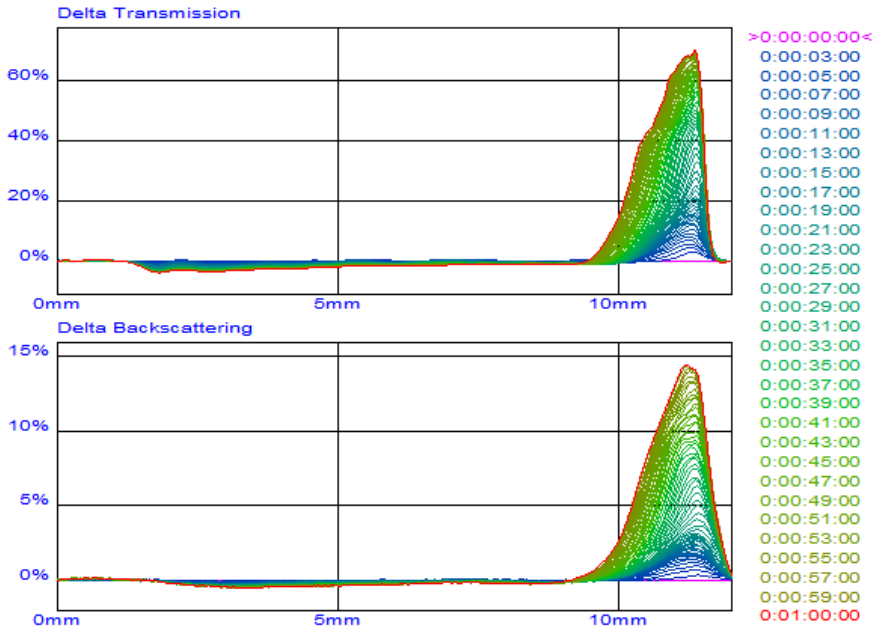

Figure 4-13 – Turbiscan Results of CNF OP

4.7. Small amplitude oscillatory shear

In order to choose an appropriate strain for the small amplitude oscillatory shear tests, the linear viscoelastic region of the suspensions must be determined first. The stress-strain curves of CNF A, B and OP are shown in Figure 4-14 to Figure 4-16, and a strain of 0.07 % was chosen based on the graphs. CNF MP was not studied due to its low performance in other characterizations.

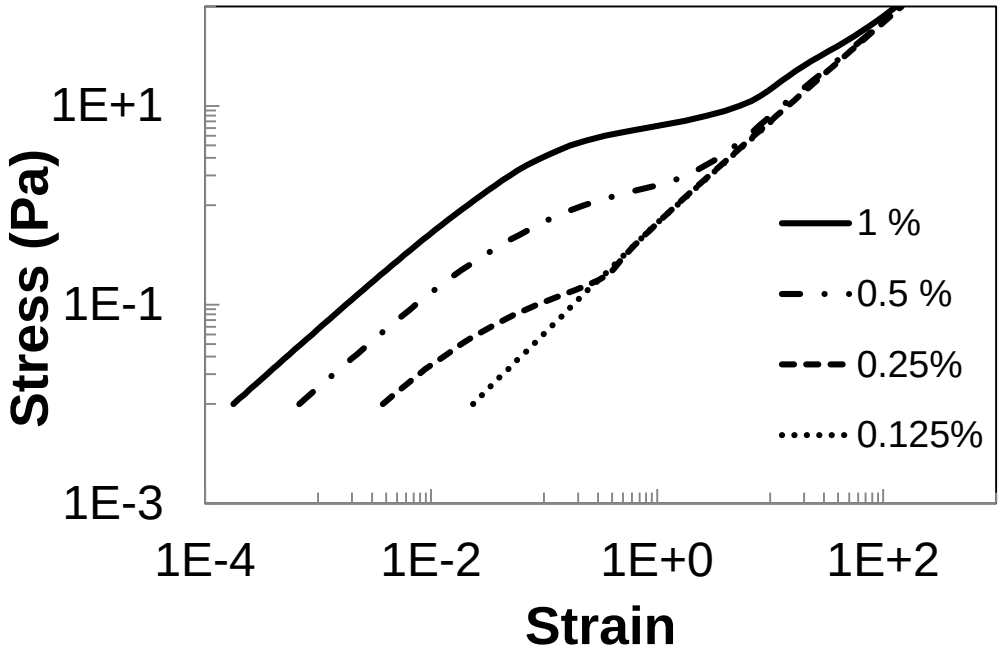

Figure 4-14 – CNF A stress vs. strain

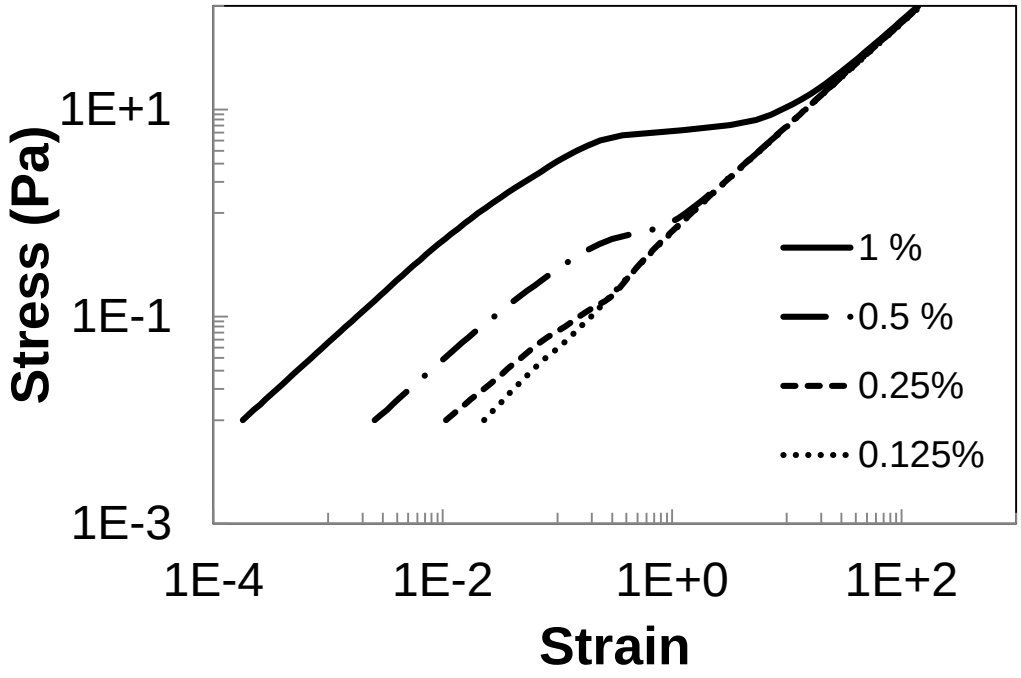

Figure 4-15 – CNF B stress vs. strain

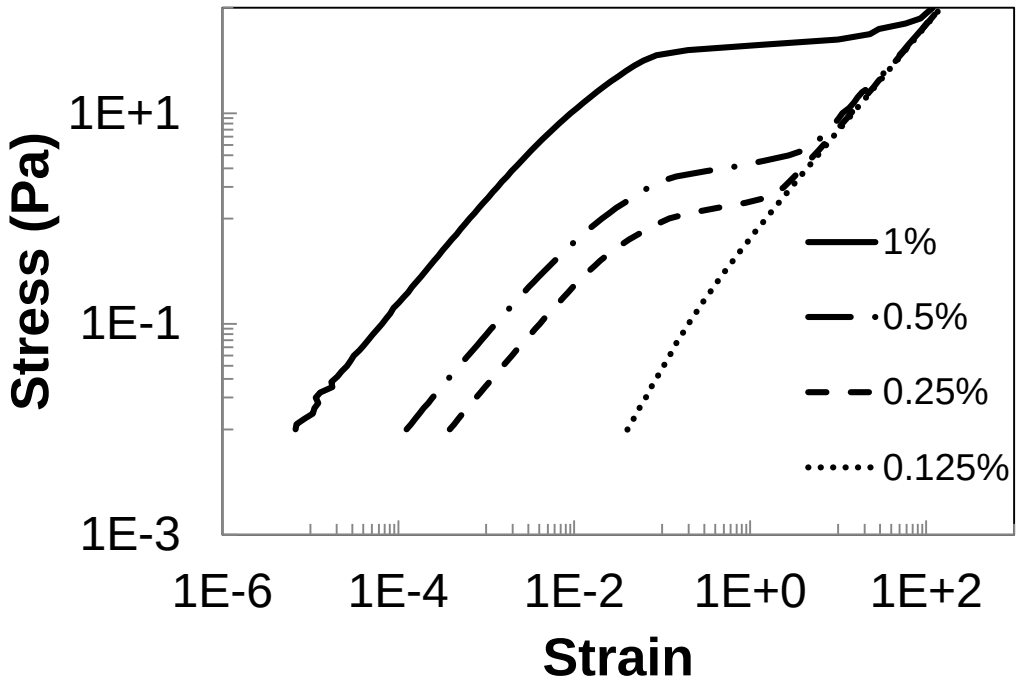

Figure 4-16 – CNF OP stress vs. strain

The storage (G') and loss moduli (G") of both CNFs are shown in Figure 4-17 to Figure 4-19.

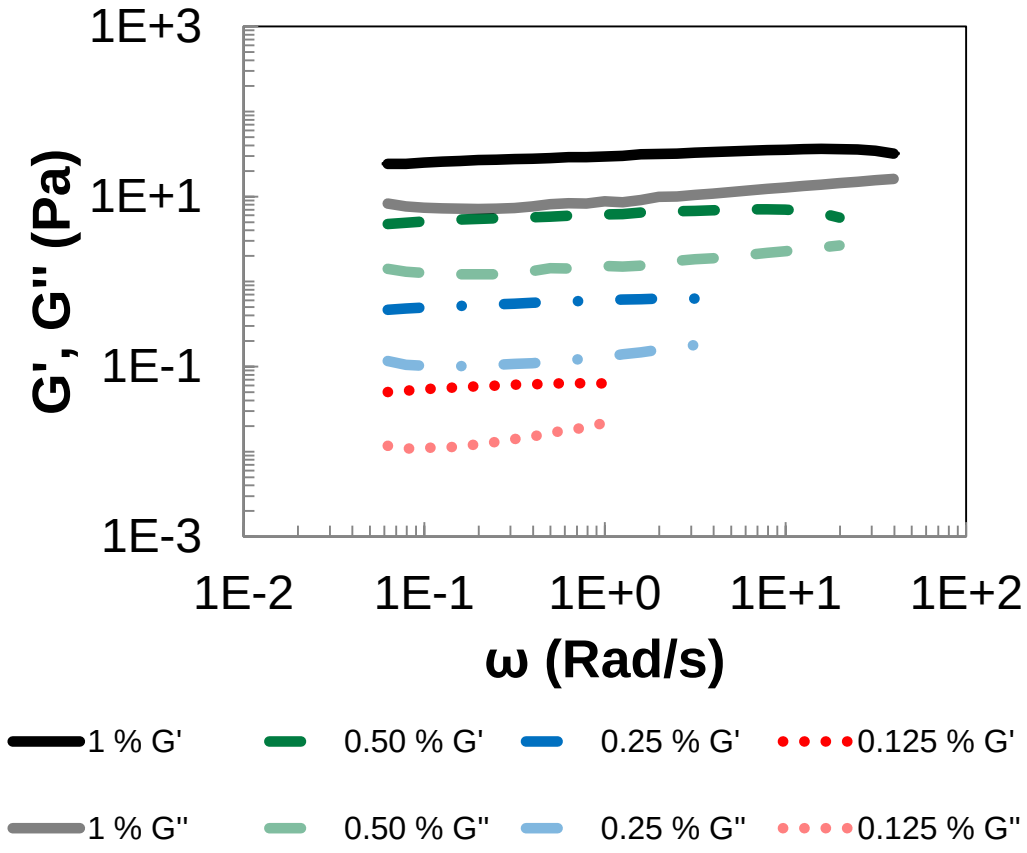

Figure 4-17 – CNF A storage and loss moduli

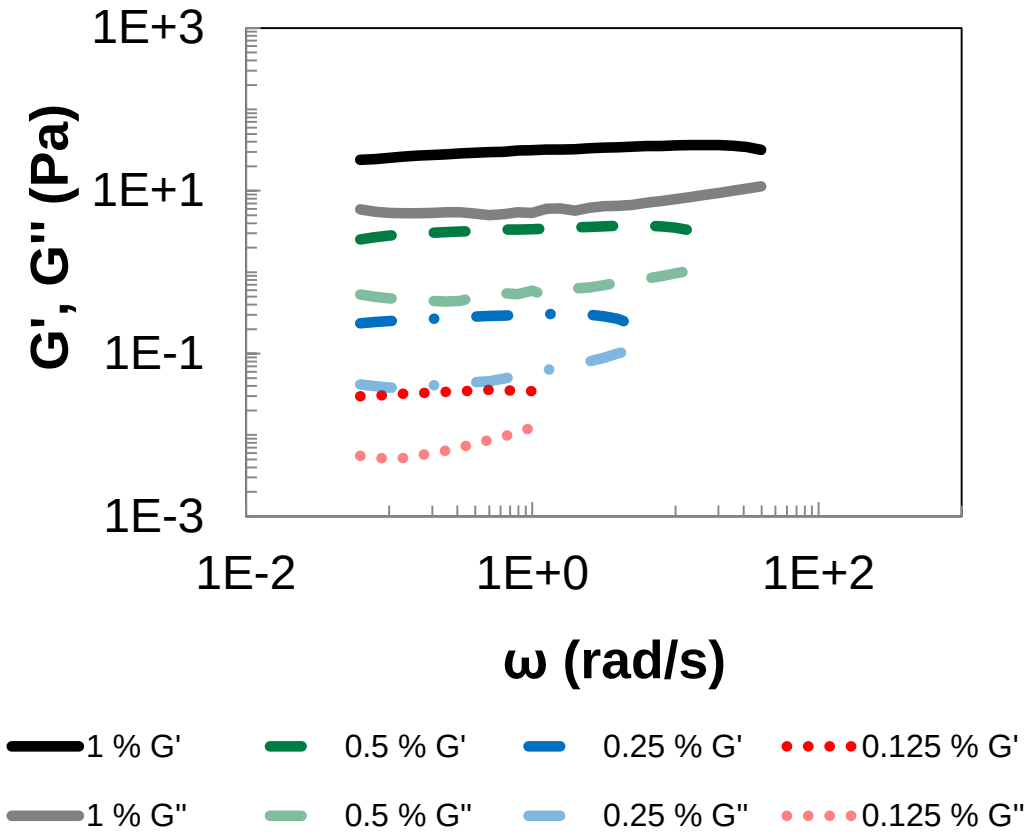

Figure 4-18 – CNF B storage and loss moduli

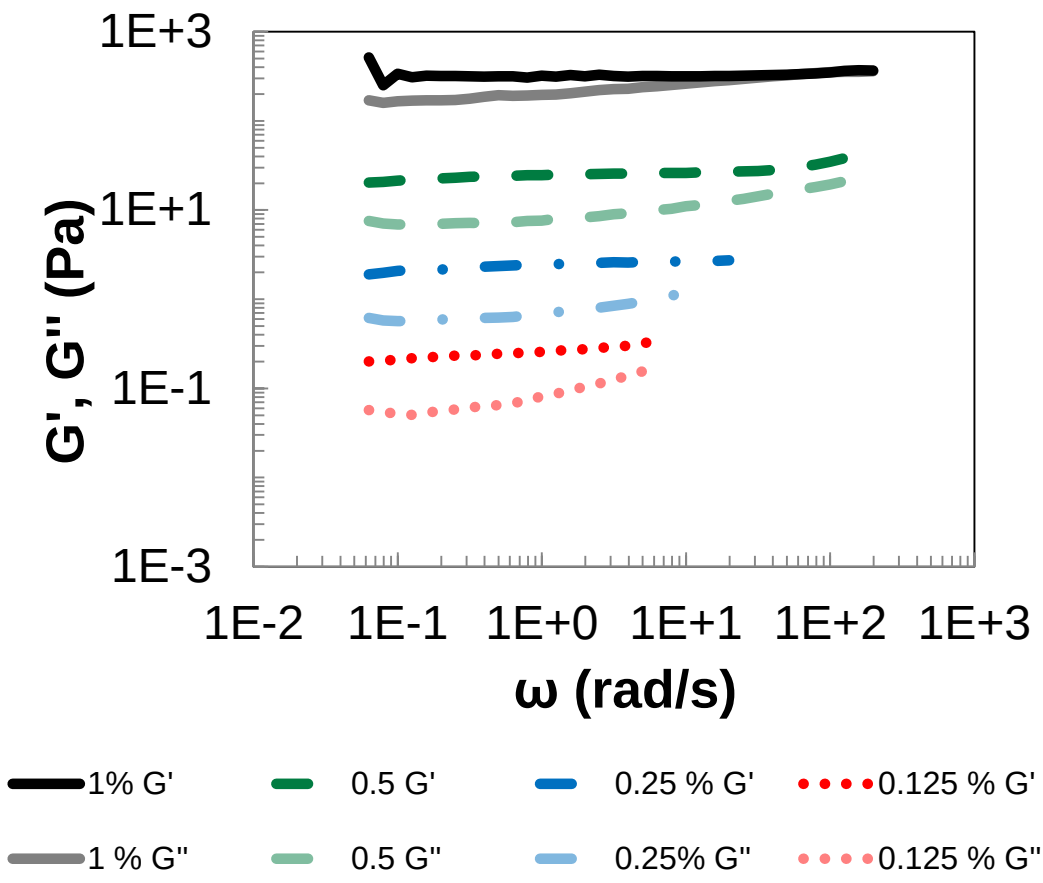

Figure 4-19 – CNF OP storage and loss moduli

For all CNFs, G' is larger than G" for all CNF concentrations. G' and G" also stay fairly constant relative to angular frequency even at the low concentration of 0.125 wt %. The G' and G" data of the commercial CNFs are in agreement with previously reported data, as they are frequency independent and G' is always larger than G", fitting the criteria for gel-like behaviour.[16] Gel-like behaviour continues to higher angular frequency with higher CNF concentrations.[16] The difference is due to more entanglement and higher interaction between CNF fibres

when there are more fibres per unit volume. The G' and G" of two commercial CNFs are similar at high (1%) concentrations, but CNF A has higher G' and G" at low (0.125 %) concentration. CNF B is in dilute regime at 0.125 wt % and CNF A is not. Thus CNF B is not able to form a network at the concentration, leading to lower G' and G". CNF OP has the highest performance in small amplitude oscillatory shear, therefore exceeding commercial varieties.

The breakdown frequency is at the end of each curve at the highest frequency. Beyond the breakdown frequency, the suspension is not able to relax to its original state and it no longer resists oscillation of the cone probe. As concentration decreases, the ability of the suspension to withstand higher angular frequency oscillation decreases. The concentration dependence is due to more entanglement of fibres at higher concentration, leading to stronger networks.

4.8. Steady state shear

The steady state rheology results are shown in Figure 4-20 to Figure 4-23.

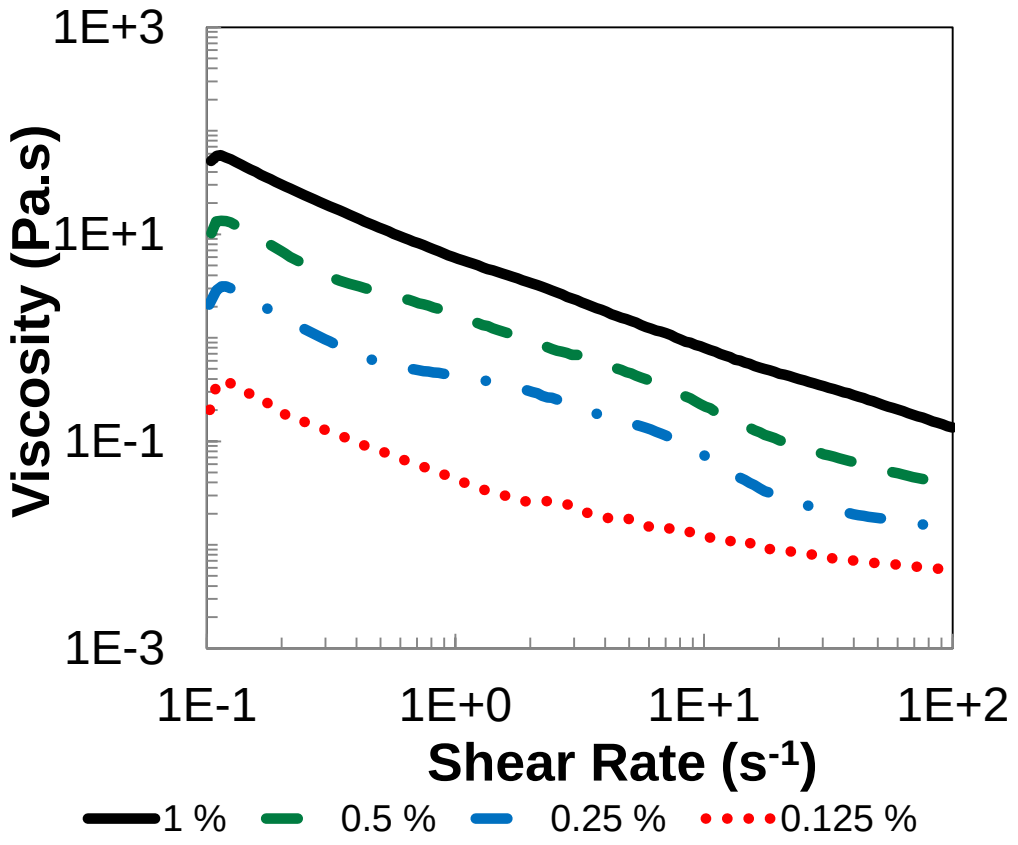

Figure 4-20 – CNF A shear viscosity in 1:1 ethylene glycol:water from 0.125 to 1 wt %

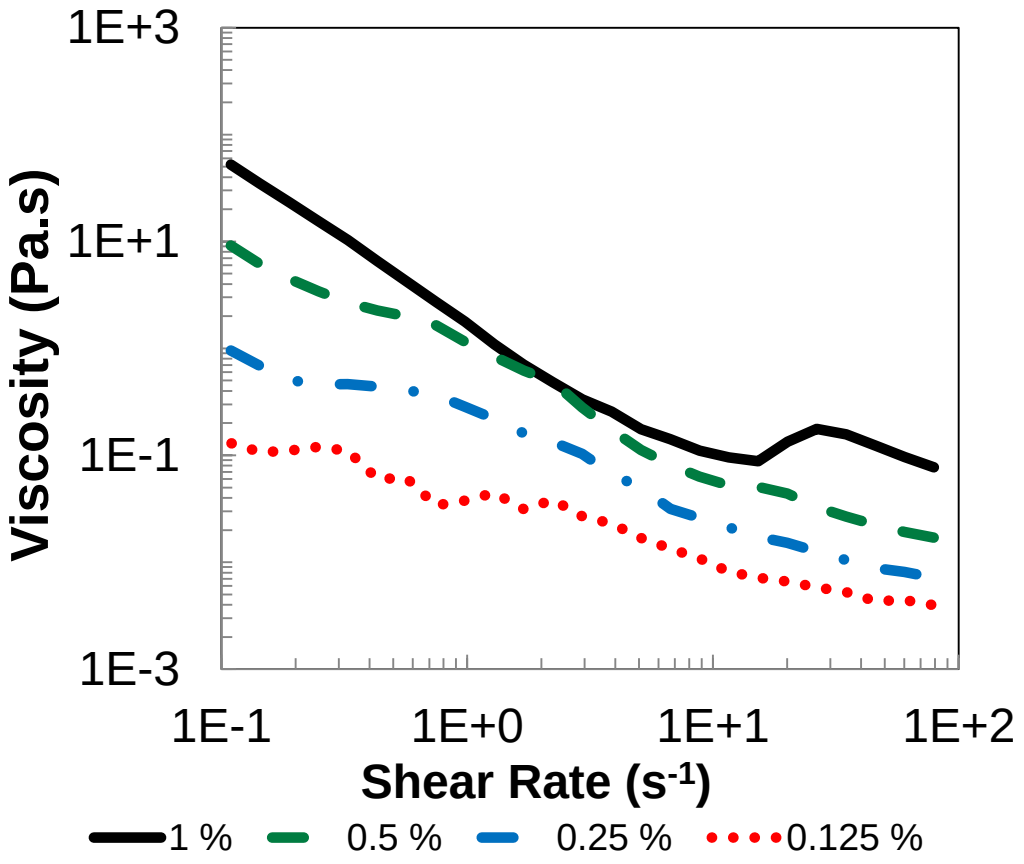

Figure 4-21 – CNF B shear viscosity in 1:1 ethylene glycol:water from 0.125 to 1 wt %

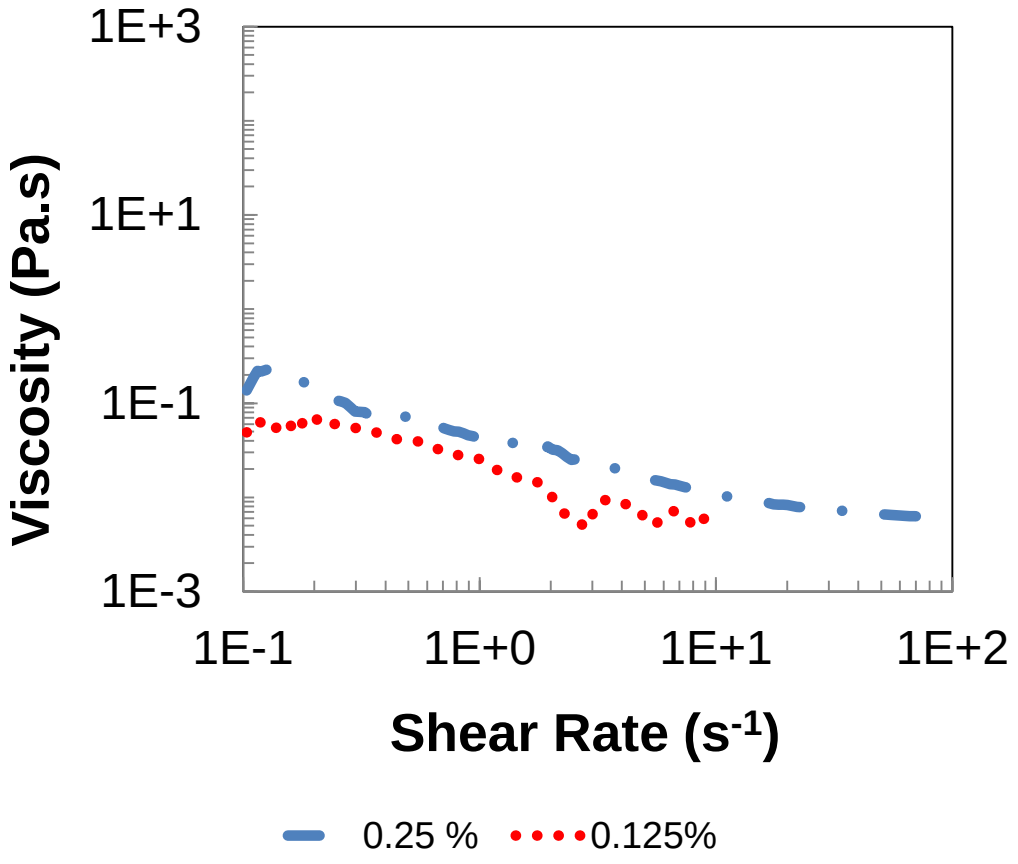

Figure 4-22 – CNF MP shear viscosity in 1:1 ethylene glycol:water from 0.125 to 0.25 wt %

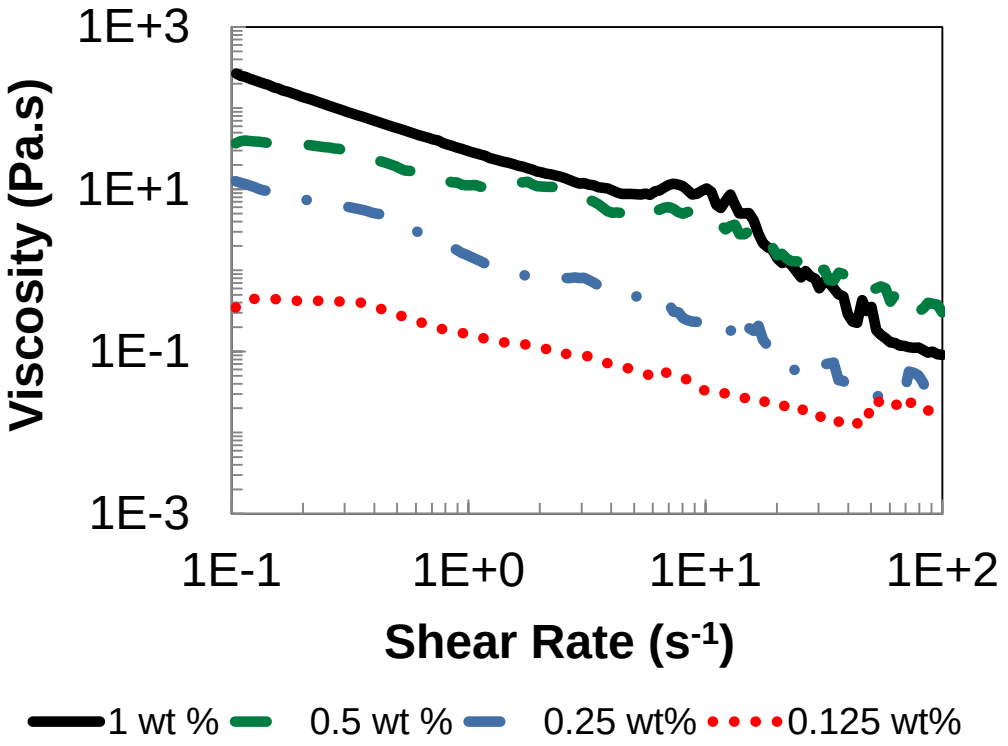

Figure 4-23 – CNF OP shear viscosity in 1:1 ethylene glycol:water from 0.125 to 1 wt %

Figure 4-22 shows only the shear viscosity at 0.25 wt % and 0.125 wt % as higher viscosities were not measured. Upon the discovery that the performance of CNF MP was inferior to commercial varieties, it was not pursued as a candidate for scale-up production.

Table 4-8 compares the relative viscosities of CNF A, B, OP and CNF from literature, and 3.9e-3 Pa.s was used as the viscosity of 1:1 ethylene:water solution at 25° C as interpolated from literature.[43]

Table 4-8 – Relative viscosities of CNF A, B, OP and literature values at 0.5 wt %

CNF Type	η_{rel} at 0.1 1/s	η_{rel} at 1 1/s	η_{rel} at 10 1/s
A	3E+3	4E+2	6E+1
B	2E+3	3E+2	1E+1
OP	9E+3	3E+3	1E+2
Literature[44]	2E+3	1E+3	1E+2

All CNF suspensions exhibit non-Newtonian behaviour down to 0.125 wt %. Shear thinning is observed for all CNF from 0.125 – 1 wt %. CNF OP the highest higher viscosity at 0.125 wt %, but CNF B shows steeper slope at 1%. Compared to CNF A, and OP CNF B has steeper slopes in viscosity vs. shear rate graphs. This means CNF B is more suitable for applications where drastic viscosity decreases are desirable with low to moderate shear rates.

The difference in shear viscosities between CNFs is more pronounced at low viscosity (0.125 wt %). Therefore, it is not enough to compare CNFs at 0.5 – 1 wt % as extrapolation to lower concentration would not be accurate, and concentration near 0.125 wt % should be studied.

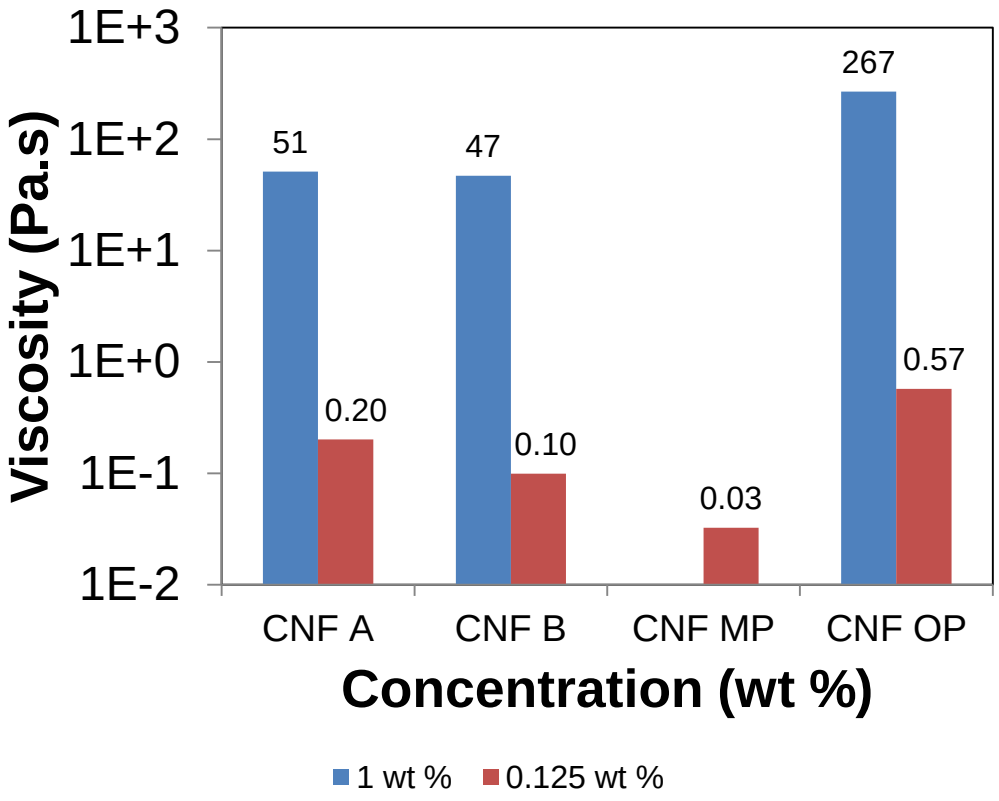

Figure 4-24 – Comparison of commercial and produced CNF viscosities at 1 and 0.125 wt % and 0.1 s^{-1} shear rate

Although the viscosity of CNF A and B at 1 wt % are very close (51 and 47 Pa.s), at 0.125 wt % CNF A is twice as viscous as CNF B. The transition into the dilute region from the semi-dilute region for CNF B above 0.125 wt % would explain this behavior. The overlap concentration of CNF B is 0.14 wt % from Table 4-5, thus at 0.125 wt % CNF B suspensions are in dilute region, whereas CNF A is still in semi-dilute region. The difference in dilute/semi-dilute regions of suspensions can account for the larger difference in viscosity at low

concentration. However, it must be noted that STEM only samples a small portion of CNF fibres and the behavior of the fibres may be different in 1:1 ethylene glycol:water, thus the overlap concentration calculated from STEM results is only a guideline and cannot be precisely applied for rheometry. When characterizing different CNFs, extrapolations of rheological data are not accurate between 0.125 to 1 wt %, since the overlap concentration may be crossed. To accurately compare the CNF rheological performances at low concentrations, a range of concentrations must be tested.

CNF B has wider diameter than CNF A based on STEM micrographs. Since CNF A is thinner and has more particles/g solution; they have higher entanglement with resulting in higher viscosity at lower concentrations. There are not enough entangled CNF B fibers at the same weight concentration to yield a smooth shear thinning curve. CNF B is thicker and stiffer. This can cause jamming at higher shear rates, seen as an increase in viscosity around 17 1/s. This jamming can be overcome when the shear rate is further increased.

The concentration dependence of shear viscosity is due to more interaction between more fibers as the concentration increases, reducing the ability to flow. At lower concentrations, a fully entangled 3D network is not formed and increasing fiber concentration increases viscosity more. At higher concentrations,

adding more fibers only reinforce the network since the network is already there; therefore the effect on viscosity is not as great.

The intrinsic viscosity can be found using the Fedors Equation, Equation (4-1),

$$\frac{1}{2(\eta_r^{1/2}-1)} = -\frac{1}{[\eta]c_m} + \frac{1}{[\eta]c} \quad \textbf{(4-1)}$$

where η_r is the relative viscosity, $[\eta]$ is the intrinsic viscocity, c_m is the maximum packing density and c is CNF concentration. Thus the intrinsic viscosity can be found by plotting the Fedors equation in Figure 4-25.

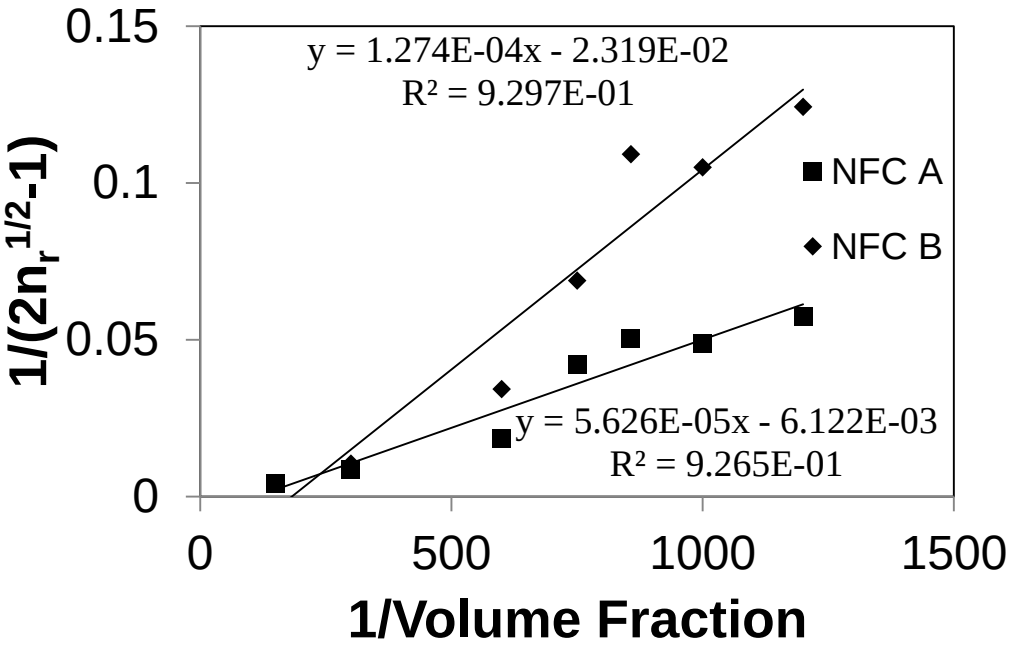

Figure 4-25 – Fedors plot of CNF A and B

Based on the trendlines in Fedors plot in Figure 4-25, the intrinsic viscosities of CNF A and B are presented in Table 4-9.

Table 4-9 – Intrinsic Viscosity of CNF A and B obtained from Fedors Plot

CNF Type	Slope	Intrinsic Viscosity	R^2
A	5.63E-05	1.77E+04	0.9265
B	1.27E-04	7.84E+03	0.9297

Equation (4-2) is the Simha equation, which relates intrinsic viscosity [η] and shape factor f, where f is length over diameter.

$$[\eta] = \frac{f^2}{15(ln2f-1.5)} + \frac{f^2}{5(ln2f-0.5)} + \frac{14}{15} \quad \textbf{(4-2)}$$

Table 4-10 – Shape factors of CNF A and B obtained from Simha equation

CNF Type	Intrinsic viscosity	Shape Factor
A	1.77E+04	652
B	7.84E+03	418

The intrinsic viscosity of CNF A is higher than CNF B. The shape factor of CNF A is also higher. Simha equation yields very high aspect ratios for both CNF. CNF A and B have very high intrinsic viscosities and shape factors.

The particle concentration per gram of CNF A and B are calculated using Equation (4-3),

$$\frac{\#\,Particle}{g\ NFC} = \frac{1}{d(\pi r^2 L)} \quad \textbf{(4-3)}$$

where d is the density of cellulose (1.5 g/cm^3), r is CNF radius, L is CNF length. The equation approximates CNF as cylindrical fibers of uniform radius. The radii used are average radii obtained from STEM. The lengths are obtained by measuring STEM micrographs as well as Simha fitting from rheological data.

Table 4-11 – Particle/weight of CNF A and B by STEM and rheology

CNF Type	# Particle/ gCNF by STEM	# Particle/ gCNF by rheology
A	1.10E+05	4.50E+04
B	2.60E+03	7.00E+02

CNF A particle concentration is higher for both methods of calculation. STEM and DLS results are based on length measurements of the main chain, whereas Simha fitting would take into account the side chains, or the interaction between chains. This difference results in a higher shape factor for rheology-based calculations. When CNF is physically crosslinked (the effective molecular weight goes up as the effective molecular weight for polymer gels is infinite).[36]

4.9. Salt effect

Electroviscous effects in CNF suspensions were studied by adding sodium chloride salt to suspensions and the results are presented in Figure 4-26.

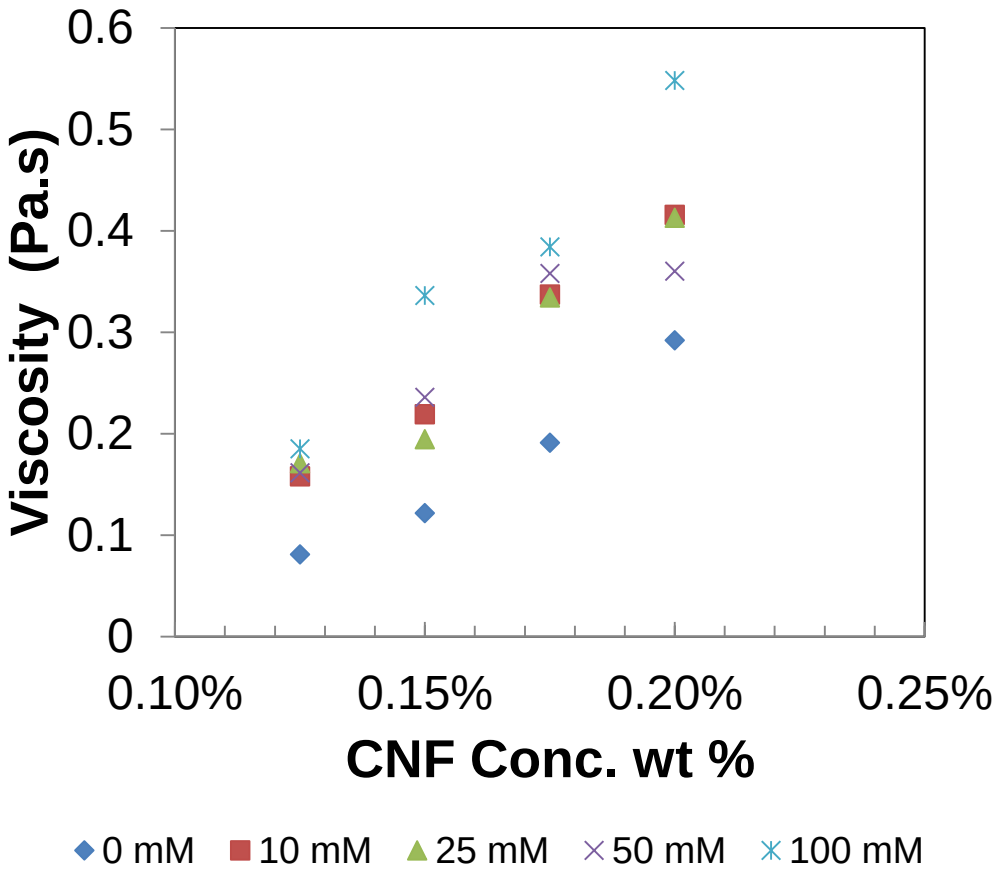

Figure 4-26 – Salt effect on CNF A viscosity

Adding salt increases the viscosity of CNF suspensions from 0.125 to 0.2 wt %, but the viscosity does not vary between 10-50 mM. At 100 mM, the viscosity increases further. Adding salt decreases electrostatic repulsion between fibres, causing higher entanglement and higher viscosity. The increase in viscosity is not as great as with CNFs with surface charge, as expected.[24]

4.10. Summary

CNF OP was produced from 4 microfluidizer passes whereas CNF MP went through 7. The white, loose fibres of CNF OP appeared more commercially desirable than the grey, caking CNF MP. STEM micrographs showed that CNF A and B were fibres with some branching and CNF OP had the smallest diameter by STEM at 42 nm. For the commercial CNFs used in this study, overlap concentrations by STEM and rheometry are in agreement. CNF's steady state and dynamic rheological performance drastically decreases below the overlap concentration.

5. Conclusions

CNF MP and OP were produced from pulp by defibrillation in a microfluidizer. CNF OP required only 4 passes in the microfluidizer, and rough estimate of its energy cost is comparable to CNF B production.

The morphology and rheological properties of CNF at low concentrations were investigated. STEM indicated high aspect ratio fibers with branches. The diameters of CNF A, B, MP, OP were 100 nm, 180 nm, 345 nm and 42 nm respectively from STEM micrographs. CNF OP showed porous and branched morphology unlike other CNFs.

CNF OP was found to have greater 5 times greater shear viscosity than commercial CNFs. Shear thinning has been observed for all CNFs for 0.125 – 1 wt %. CNF B is more shear thinning at 1 wt %, making it more suitable for applications where a much lower processing viscosity is required. CNF OP performed better than CNF A, B in small amplitude oscillatory shear rheology. The storage and loss moduli were all fairly independent of oscillation frequency, and storage moduli were always larger than loss modulus all concentrations tested. This implies that all CNFs tested behave like gels. Adding NaCl increases CNF suspension viscosity due to decrease in electrostatic repulsion.

CNF OP is an excellent candidate for a viscosity modifier due to its superior rheological performance and appearance. The low energy input in production of CNF OP makes it also suitable for scale-up production. CNF MP did not perform as well as commercial samples, thus it is not suitable as a co-product in the Bioconversion Network as such.

6. Future work

The future work suggested includes characterizing the long term stability of CNF, other beneficial characteristics of CNF, study of CNF applications, scale-up production optimization and integration with the biorefinery process.

Although the performance of CNF MP did not measure up to commercial samples or CNF OP, STEM micrographs did show some finely defibrillated fibres. The lignin in MP hinders mechanical defibrillation, which resulted in some large unfibrillated chunks that decreased performance. If an additional delignification step is added to MP production, the performance of MP is expected to go up. Since MP is a waste product from enzymatic hydrolysis, utilizing this waste would be highly beneficial to the bioconversion process.

The colloidal stability of CNF was studied over 1 hour in at 0.125 wt % in 1:1 Ethylene Glycol:Water. The settling would decrease in application, as the viscosity would be higher, but a longer stability study may be needed to ensure it is acceptable before the material dries or is used. The long-term storage of CNF should also be studied to determine if biodegradation occurs. CNF OP did not degrade after 2 months while stored at 4 °C. A biocide may need to be added to the formulation to prevent biodegradation, especially if formulations with CNF have to be stored at room temperature.

This study focussed on producing CNF as a viscosity modifier. CNF has other properties that can be explored, such modification of adhesive properties, mechanical strength and water retention.

In the future, the performance of CNF in cement, paint, personal care products and other applications can be studied. The interaction of CNF and practical formulations need to be studied comprehensively, and this can be done in collaboration with a commercial partner. The improvement of rheological properties at rest and during processing should be studied, and other properties mentioned above can also be studied in commercial products.

The production of CNF has been optimized with the equipment available, but it is only at a smaller scale. The microfluidizer used in this thesis is the M-110EH-30, which is suitable for lab and pilot scale projects. Microfluidics Corporation also offers the M-700 series processors, suitable for larger production scale environments. The production cost is expected to decrease with a larger scale production.

CNF was produced within the NSERC Bioconversion Network and Integration with the bioconversion process is expected. The Bioconversion Network can provide expertise and raw materials for CNF production. CNF will bring revenue while having the same pretreatment process for ethanol and CNF production can

lower CNF production costs. Working in close collaboration with Bioconversion Network Theme 1 – Pretreatment and Theme 4 – Optimization would help streamline the process. Additionally, partnering with Alberta Innovates – Technology Futures would provide pilot plant facilities and production expertise. Once successful, CNF production can bring new revenues to the forestry industry and support the green fuel revolution.

7. References

1. Klemm, D.; Heublein, B.; Fink, H. P.; Bohn, A., Cellulose: Fascinating biopolymer and sustainable raw material. *Angewandte Chemie - International Edition* **2005,** *44* (22), 3358-3393.

2. Klemm, D., Nanocelluloses: A New Family of Nature-Based Materials. *Angewandte Chemie International Edition* **2011,** *50* (24), 5438-5466.

3. Hinterstoisser, B.; Åkerholm, M.; Salmén, L., Load distribution in native cellulose. *Biomacromolecules* **2003,** *4* (5), 1232-1237.

4. Henriksson, G.; Gellerstedt, G.; Ek, M., Pulp and Paper Chemistry and Technology. Volume 1, Wood Chemistry and Wood Biotechnology. Walter de Gruyter: 2009.

5. Salmén, L., Micromechanical understanding of the cell-wall structure. *Comptes Rendus Biologies* **2004,** *327* (9–10), 873-880.

6. Herráez-Domínguez, J. V.; de León, F. G. G.; Díez-Sales, O.; Herráez-Domínguez, M., Rheological characterization of two viscosity grades of methylcellulose: An approach to the modeling of the thixotropic behaviour. *Colloid and Polymer Science* **2005,** *284* (1), 86-91.

7. Lee, J. W., Advanced Biofuels and Bioproducts. Springer: 2012.

8. Toppinen, A.; Zhang, Y.; Geng, W.; Laaksonen-Craig, S.; Lahtinen, K.; Li, N.; Liu, C.; Majumdar, I.; Shen, Y. Changes in Global Markets for Forest

Products and Timberlands. www.iufro.org/download/file/5895/4668/135-156_pdf (accessed 19/08/2013).

9. Hurmekoski, E.; Hetemäki, L., Studying the future of the forest sector: Review and implications for long-term outlook studies. *Forest Policy and Economics* **2013,** *34* (0), 17-29.

10. Turbak, A. F., Microfibrillated cellulose--a new composition of commercial significance. 1984.

11. Olszewska, A.; Eronen, P.; Johansson, L. S.; Malho, J. M.; Ankerfors, M.; Lindström, T.; Ruokolainen, J.; Laine, J.; Österberg, M., The behaviour of cationic NanoFibrillar Cellulose in aqueous media. *Cellulose* **2011,** *18* (5), 1213-1226.

12. TAPPI Roadmap for the Development of International Standards for Nanocellulose. http://www.tappinano.org/pdf/RoadmapforNanocelluloseStandards.pdf (accessed 12/02/13).

13. NSERC Bioconversion Network. http://www.nsercbioconversion.net/ (accessed 04/08/2013).

14. Zhu, J. Y.; Sabo, R.; Luo, X., Integrated production of nano-fibrillated cellulose and cellulosic biofuel (ethanol) by enzymatic fractionation of wood fibers. *Green Chemistry* **2011,** *13* (5), 1339-1344.

15. Kim, C. F., M.; Marquez, M. Joo, Y. L., Preparation of Submicron-Scale, Electrospun CelluloseFibers via Direct Dissolution. *Journal of Polymer Science, Part B: Polymer Physics* **2005,** *43* (13), 1673-1683.

16. Paakko, M.; Ankerfors, M.; Kosonen, H.; Nykanen, A.; Ahola, S.; Ostenberg, M.; Ruokalainen, J.; Laine, J.; Larsson, P. T.; Ikkala, O.; Lindström, T., Enzymatic Hydrolysis Combined with Mechanical Shearing and High Pressure Homogenization for Nanoscale Cellulose Fibrils. *Biomacromolecules* **2007,** *8* (6), 1934-1941.

17. Miao, C.; Hamad, W. Y., Cellulose reinforced polymer composites and nanocomposites: a critical review. *Cellulose* **2013**, 1-42.

18. Korhonen, J. T.; Kettunen, M.; Ras, R. H. A.; Ikkala, O., Hydrophobic nanocellulose aerogels as floating, sustainable, reusable, and recyclable oil absorbents. *ACS Applied Materials and Interfaces* **2011,** *3* (6), 1813-1816.

19. Faraco, V., Lignocellulose Conversion: Enzymatic and Microbial Tools for Bioethanol Production. Springer London, Limited: 2013.

20. Atalla, R. H.; VanderHart, D. L., The role of solid state 13C NMR spectroscopy in studies of the nature of native celluloses. *Solid State Nuclear Magnetic Resonance* **1999,** *15* (1), 1-19.

21. Šturcová, A.; His, I.; Apperley, D. C.; Sugiyama, J.; Jarvis, M. C., Structural Details of Crystalline Cellulose from Higher Plants. *Biomacromolecules* **2004,** *5* (4), 1333-1339.

22. Lavoine, N.; Desloges, I.; Dufresne, A.; Bras, J., Microfibrillated cellulose - Its barrier properties and applications in cellulosic materials: A review. *Carbohydrate Polymers* **2012,** *90* (2), 735-764.

23. Eyholzer, C.; Bordeanu, N.; Lopez-Suevos, F.; Rentsch, D.; Zimmermann, T.; Oksman, K., Preparation and characterization of water-redispersible nanofibrillated cellulose in powder form. *Cellulose* **2010,** *17* (1), 19-30.

24. Fall, A. B.; Lindström, S. B.; Sprakel, J.; Wågberg, L., A physical cross-linking process of cellulose nanofibril gels with shear-controlled fibril orientation. *Soft Matter* **2013,** *9* (6), 1852-1863.

25. Saito, T.; Nishiyama, Y.; Putaux, J. L.; Vignon, M.; Isogai, A., Homogeneous suspensions of individualized microfibrils from TEMPO-catalyzed oxidation of native cellulose. *Biomacromolecules* **2006,** *7* (6), 1687-1691.

26. Abraham, E. e. a., Extraction of nanocellulose fibrils from lignocellulosic fibres: a novel approach. *Carbohydrate Polymers* **2011,** *86* (4), 1468-1475.

27. Liu, H. H., Y., Ultrafine Fibrous Cellulose Membranes from Electrospinning of Cellulose Acetate. *Journal of Polymer Science, PartB: Polymer Physics* **2002,** *40* (18), 2119-2129.

28. Brown Jr, R. M.; Barnes, Z.; Sawatari, C.; Kondo, T., Polymer manipulation and nanofabrication in real time using transmission electron microscopy. *Biomacromolecules* **2007,** *8* (1), 70-76.

29. Krishnamachari, P.; Hashaikeh, R.; Tiner, M., Modified cellulose morphologies and its composites; SEM and TEM analysis. *Micron* **2011,** *42* (8), 751-761.

30. Michael, G. H., Electron Microscopy of Polymers. Springer: 2008; p. 473. (accessed Dec 16th, 2012).

31. Ying, Q.; Marecek, J.; Chu, B., Solution behavior of buckminsterfullerene (C60) in benzene. *Journal of Chemical Physics* **1994,** *101* (4), 2665-2672.

32. Williams, D. B.; Carter, C. B., Transmission Electron Microscopy: A Textbook for Materials Science. Diffraction. II. Springer: 1996.

33. Boluk, Y.; Lahiji, R.; Zhao, L.; McDermott, M. T., Suspension viscosities and shape parameter of cellulose nanocrystals (CNC). *Colloids and Surfaces A: Physicochemical and Engineering Aspects* **2011,** *377* (1-3), 297-303.

34. Fall, A. B.; Lindström, S. B.; Sundman, O.; Ödberg, L.; Wågberg, L., Colloidal stability of aqueous nanofibrillated cellulose dispersions. *Langmuir* **2011,** *27* (18), 11332-11338.

35. Celia, C.; Trapasso, E.; Cosco, D.; Paolino, D.; Fresta, M., Turbiscan Lab® Expert analysis of the stability of ethosomes® and ultradeformable liposomes containing a bilayer fluidizing agent. *Colloids and Surfaces B: Biointerfaces* **2009,** *72* (1), 155-160.

36. Grillet, A. M.; Wyatt, N. B.; Gloe, L. M., Polymer Gel Rheology and Adhesion. In *Rheology*, De Vicente, J., Ed. InTech: 2012.

37. Iotti, M.; Gregersen, Ø. W.; Moe, S.; Lenes, M., Rheological Studies of Microfibrillar Cellulose Water Dispersions. *J Polym Environ* **2011,** *19* (1), 137-145.

38. Pan, X.; Xie, D.; Yu, R. W.; Saddler, J. N., The bioconversion of mountain pine beetle-killed lodgepole pine to fuel ethanol using the organosolv process. *Biotechnology and Bioengineering* **2008,** *101* (1), 39-48.

39. Sluiter, A.; Hames, B.; Ruiz, R.; Scarlata, C.; Sluiter, J.; Templeton, D.; Crocker, D., Determination of structural carbohydrates and lignin in biomass. *Laboratory Analytical Procedure* **2008**.

40. Panagiotou, T. M. Microfluidizer® Processors: Technology and Applications. http://www.bio.huji.ac.il/upload/Cellular_Microfluidizer_Protocols.pdf (accessed 17//06/13).

41. Innventia Nanocellulose - Innventia. http://www.innventia.com/en/Our-Expertise/New-materials/Nanocellulose (accessed 01/08/2013).

42. Utilities Consumer Advocate: Price Summary. http://www.ucahelps.alberta.ca/price-summary.aspx.

43. Sun, T.; Teja, A. S., Density, Viscosity, and Thermal Conductivity of Aqueous Ethylene, Diethylene, and Triethylene Glycol Mixtures between 290 K and 450 K. *Journal of Chemical & Engineering Data* **2002,** *48* (1), 198-202.

44. Agoda-Tandjawa, G.; Durand, S.; Berot, S.; Blassel, C.; Gaillard, C.; Garnier, C.; Doublier, J. L., Rheological characterization of microfibrillated

cellulose suspensions after freezing. *Carbohydrate Polymers* **2010,** *80* (3), 677-686.